repositorio institucional IMDEA Nanociencia

Optical properties and plasmons in moiré structures

Xueheng Kuang, Pierre A Pantaleón Peralta, Jose Angel Silva-Guillén, Shengjun Yuan, Francisco Guinea and Zhen Zhan

This is the Accepted Manuscript version of an article accepted for publication in Journal of Physics: Condensed Matter. IOP Publishing Ltd is not responsible for any errors or omissions in this version of the manuscript or any version derived from it. The Version of Record is available online at https://iopscience.iop.org/article/10.1088/1361-648X/ad1f8c.

To cite this version

Xueheng Kuang, Pierre A Pantaleón Peralta, Jose Angel Silva-Guillén, Shengjun Yuan, Francisco Guinea and Zhen Zhan. Optical properties and plasmons in moiré structures. 2024. https://hdl.handle.net/20.500.12614/3593

Licensing

Use of this Accepted Version is subject to the publisher's Author Rights terms of use https://publishingsupport.iopscience.iop.org/author-rights-policies/

This Accepted Manuscript is available for reuse under a CC BY-NC-ND licence after the 12 month embargo period provided that all the terms of the licence are adhered to

Embargo

This version (post-print or accepted manuscript) of the article has been deposited in the Institutional Repository of IMDEA Nanociencia with an embargo lifting on 31.01.2025.

Optical properties and plasmons in moiré structures

Xueheng Kuang

Yangtze Delta Industrial Innovation Center of Quantum Science and Technology, Suzhou 215000, China

Pierre A. Pantaleón Peralta

Instituto Madrileño de Estudios Avanzados, IMDEA Nanociencia, Calle Faraday 9, 28049, Madrid, Spain

Jose Angel Silva-Guillén

Instituto Madrileño de Estudios Avanzados, IMDEA Nanociencia, Calle Faraday 9, 28049, Madrid, Spain

Shengjun Yuan

Key Laboratory of Artificial Micro- and Nano-structures of the Ministry of Education and School of Physics and Technology, Wuhan University, Wuhan 430072, China
Wuhan Institute of Quantum Technology, Wuhan 430206, China

Francisco Guinea

Instituto Madrileño de Estudios Avanzados, IMDEA Nanociencia, Calle Faraday 9, 28049, Madrid, Spain
Donostia International Physics Center, Paseo Manuel de Lardizábal 4, 20018, San Sebastián, Spain

Zhen Zhan

Instituto Madrileño de Estudios Avanzados, IMDEA Nanociencia, Calle Faraday 9, 28049, Madrid, Spain

E-mail: zhenzhanh@gmail.com

November 2023

Abstract. The discoveries of numerous exciting phenomena in twisted bilayer graphene (TBG) are stimulating significant investigations on moiré structures that possess a tunable moiré potential. Optical response can provide insights into the electronic structures and transport phenomena of non-twisted and twisted moiré structures. In this article, we review both experimental and theoretical studies of optical properties such as optical conductivity, dielectric function, non-linear optical response, and plasmons in moiré structures composed of graphene, hexagonal boron nitride (hBN), and/or transition metal dichalcogenides (TMDCs). Firstly, a comprehensive introduction to the widely employed methodology on optical properties is presented. After, Moiré potential induced optical conductivity and plasmons in non-twisted structures are reviewed, such as single layer graphene-hBN, bilayer graphene-hBN and graphene-TMDCs moiré heterostructures. Next, recent investigations of twist-angle dependent optical response and plasmons are addressed in twisted moiré structures. Additionally, we discuss how optical properties and plasmons could contribute to the understanding of the many-body effects and superconductivity observed in moiré structures.

Keywords: moiré structures, optical conductivity, plasmons,twisted bilayer graphene

1. Introduction

Two-dimensional (2D) materials, such as graphene [1], hexagonal boron nitride (hBN) [2, 3], transition metal dichalcogenides (TMDCs) [4, 5] and many others [6, 7], have been widely investigated over the past two decades [8]. The fact that the isolated atomic planes could be stacked layer by layer via weak van der Waals interactions, forming moiré structures, provides an avenue to realize functionalities distinct from the components of the moiré systems [9]. Interestingly, heterostructures of two materials with different lattice constants form large-scale structures that display a moiré pattern, which we will refer to as non-twisted moiré structures. For example, by depositing graphene on top of hBN, if they are aligned, we would obtain a graphene-hBN moiré structure with a moiré length of around 14 nm [10]. Moiré structures can also be obtained by rotating two layers with a relative twist angle, which are commonly known as twisted moiré structures [11, 12]. Twisted moiré structures have attracted tremendous attentions due to the emergence of a rich phase diagram of correlated states. For instance, in twisted bilayer graphene (TBG), when two graphene layers are rotated by an angle of 1.05°, known as the magic angle, flat bands appear at the charge neutrality point [13, 14]. As a consequence, exotic phenomena are observed, ranging from unconventional superconductivity [15–17] to correlated insulator phases [18–22], topological Chern insulators [23, 24], ferromagnetism [25–27], anomalous Hall effects [26, 28, 29] and non-linear Hall effects [30]. These findings have also motivated further search of electronic flat bands in other twisted moiré structures like twisted trilayer graphene (TTG) [31–33], twisted double bilayer graphene (TDBG) [34–37], twisted bilayer TMDCs [38–44], twisted bilayer hBN [45–48], and so on. In fact, correlated insulators and tunable superconductivity have also been found in twisted multilayer graphene systems [49–58]. Emergence of flat bands can also induce orbital ferromagnetism and correlated insulator states in non-twisted moiré structures such as aligned trilayer ABC graphene-hBN [59–62], and hBN-graphene-hBN heterostructures [63]. On the other hand, twisted bilayer TMDCs can also be exceptional frameworks for investigating many-body insulators [64, 65], Hubbard physics [66, 67] and the quantum anomalous Hall effect [68–71]. More importantly, large-scale moiré structures also enables exciting photonic and optoelectronic properties, like moiré excitons [72] and polaritons as, reviewed in [73].

In the search for downscaling technological devices, optical properties, such as optical conductivity [74–76], dielectric function [77–80], etc. have been extensively explored in 2D materials. The unique electronic structure of graphene has motivated research focused on the fields of non-linear plasmon response [81], plasmon-polariton [82,83], and other plasmonics [84]. From the perspective of applications, graphene stands out to be a very promising candidate for terahertz to mid-infrared applications [85], such as modulators, polarizers, mid-infrared photodetectors or mid-infrared vibrational spectroscopy [86, 87]. Furthermore, to make significant advances in the confinement of light, plasmons have been extensively studied in graphene and TMDCs and have

been shown to have potential applications for the development of new state-of-the-art optical devices [86, 88–92]. From a fundamental point of view, the optical and plasmon properties of 2D materials are extremely sensitive to their band structure. Thus, the optical properties could shed light on electronic structure [93], which could serve to further investigate exotic quantum phases. Since moiré structures can exhibit distinct electronic properties from their building block counterparts, moiré structures such as TBG can lead to numerous exciting optical phenomena and could be used in future generations of optoelectronic devices [94,95]. Here, we present an overview of the recent progress in the matter of emerging linear optical response, plasmons and their relations to other interesting properties in both non-twisted and twisted moiré structures.

This review is organized as follows: Section 2 introduces the common experimental and theoretical methods for investigating optical properties and plasmons. Optical properties and plasmons are described for non-twisted moiré structures, and for twisted moiré structures in Sections 3 and 4, respectively. The relation to other properties such as many-body effects and superconductivity, and a brief description of the non-linear optical response are discussed in Section 5. In Section 6 we give a final summary and future perspectives.

2. Methodology

This section is devoted to the introduction of the experimental techniques and theoretical framework that are needed to study the linear optical response of moiré structures.

2.1. Experimental techniques

In general, 2D materials and 2D material-based moiré structures are expected to show strong light-matter interaction and enriched photoresponses. For 2D systems, the response to an applied electromagnetic field can be mainly characterized by the optical conductivity, $\sigma(\omega)$. Since the optical conductivity is uniquely determined by the band structure, it is a powerful tool to understand the electronic properties of ~~2D~~ materials. Experimentally, infrared spectroscopy (IR) is a widely used technique to measure the optical conductivity of a material [86]. Another promising technique is the scattering-type scanning near-field optical microscope (s-SNOM) [96], which could provide the propagation of the surface plasmons by measuring the scattering amplitude $S_{opt}(x)$. The advantage of the s-SNOM is that, from the plasmon dispersion, it is possible to extract the optical conductivity $\sigma(\omega)$ and loss function $S(\mathbf{q},\omega)$, enabling experimental access to both the electronic band structure and electron-hole excitations of the systems [97, 98]. Electron energy-loss spectroscopy (EELS) has also advanced in recent decades to provide the structural and optical characterization of materials by correlating the acquired infrared-to-ultraviolet spectral data with morphological and structural information derived from secondary electron images (in scanning electron microscope (SEM)) or the high-angle annular dark-field signal (in transmission electron

microscope (TEM)) [99]. The loss function $S(\mathbf{q},\omega)$ can be extracted from the EELS spectra. Currently, the measured results are a collection of signals from large area samples, which are unable to provide the local structure of the moiré system and could be influenced by extrinsic effects, for example, twist angle inhomogeneities or strain present in the sample. Thanks to the development of new techniques, such as 4D scanning TEM spectroscopy [100] and near-field scanning [101], it is possible to locally probe the optoelectronic properties and could be used to study the properties of moiré structures.

2.2. Theoretical methods

Concerning the theoretical approach, through linear response theory, we can obtain optical properties by calculating different response functions. For example, the optical conductivity $\sigma(\omega)$, and the polarization function $\Pi_0(\mathbf{q},\omega)$ are evaluated from the current-current and non-interacting density-density response functions, respectively. Other optical properties such as the dielectric function $\varepsilon(\mathbf{q},\omega)$, loss function $S(\mathbf{q},\omega)$ and the optical absorption coefficient can be extracted from those quantities, as discussed below.

2.2.1. Linear optical response The optical conductivity can be derived using the Kubo formula [102] and can be written as the Kubo-Greenwood equation [103]

$$\sigma_{\alpha 1\alpha 2}(\omega)=\frac{g_s i}{(2\pi)^D}\int_{BZ}d^Dk\sum_{l,l'}\frac{n_F\left(E_{\boldsymbol{k}l'}\right)-n_F\left(E_{\boldsymbol{k}l}\right)}{E_{\boldsymbol{k}l}-E_{\boldsymbol{k}l'}}\frac{\left\langle \boldsymbol{k}l'\left|J_{\alpha 1}\right|\boldsymbol{k}l\right\rangle\left\langle \boldsymbol{k}l\left|J_{\alpha 2}\right|\boldsymbol{k}l'\right\rangle}{E_{\boldsymbol{k}l'}-E_{\boldsymbol{k}l}+\hbar\omega+i\delta}, \tag{1}$$

where g_s is the spin degeneracy, D is the dimension of moiré structures and is typically set to 2 for 2D materials. $J_{\alpha 1}$ and $J_{\alpha 2}$ are current operators along the $\alpha 1$ and $\alpha 2$ directions, respectively. n_F is the Fermi-Dirac distribution. Eigenvalues, $E_{\boldsymbol{k}l}$, and eigenstates, $|\boldsymbol{k}l\rangle$, with band index l and momentum $\boldsymbol{k}$, are needed to describe optical band transitions between l and l' bands. The integration runs over the whole Brillouin zone (BZ).

By combining the Kubo formula with the tight-binding propagation method (TBPM), the optical conductivity (omitting the Drude contribution at $\omega=0$) could be expressed as [104, 105]

$$\begin{aligned}\sigma_{\alpha 1\alpha 2}(\omega)=\lim_{\varepsilon\to 0^+}\frac{e^{-\beta\hbar\omega}-1}{\hbar\omega\Omega}\int_0^\infty e^{-\varepsilon t}\left(\sin\omega t-i\cos\omega t\right)\\ \times 2\mathrm{Im}\left\{\left\langle\varphi\left|n_F(H)\,e^{iHt}J_{\alpha 1}e^{-iHt}[1-n_F(H)]J_{\alpha 2}\right|\varphi\right\rangle\right\}dt,\end{aligned} \tag{2}$$

where Ω is the area of the system, $\beta=1/(k_BT)$ being k_B the Boltzmann constant, H is the Hamiltonian, and $|\varphi\rangle$ is the initial state of the system, which is a random superposition of all basis states

$$|\varphi\rangle=\sum_i a_i|i\rangle, \tag{3}$$

where $|i\rangle$ are all basis states in real space and a_i are random complex numbers normalized as $\sum_i|a_i|^2=1$.

The calculation of equation (2) scales linearly with the number of states N of the system in real space. In contrast, the scaling would be $O(N^3)$ if we were to solve equation (1) using the exact diagonalization method to obtain the eigenstates and eigenvalues of the system. Therefore, calculating the optical conductivity using equation (2) has advantages when dealing with non-periodic moiré structures, such as 30° dodecagonal graphene quasicrystal [106–110] and large-scale periodic moiré structures [105]. Interestingly, disorder effects on optical conductivity can be also easily be considered with this real-space method [111]. It is important to note that there are similar real-space methods with $O(N)$ time scaling that do not require time propagation to calculate transport conductivity $\sigma_{\alpha\beta}(\omega = 0)$ [112, 113].

The optical conductivity corresponds to the optical absorption spectrum that can be extracted from raw data of IR using multilayer Kramers-Kronig analysis program [114], and is related to the transmission of incident light perpendicular to the system, which is given by [115]

$$T = |1 + \frac{2\pi}{c}\sigma(\omega)|^{-2} \approx 1 - \frac{4\pi}{c}\mathrm{Re}\left\{\sigma(\omega)\right\}. \tag{4}$$

Absorbance at normal incidence could be expressed as [75]

$$A = \frac{4\pi}{c}\mathrm{Re}\left\{\sigma(\omega)\right\}, \tag{5}$$

where $\mathrm{Re}\left\{\sigma(\omega)\right\}$ is the real part of optical conductivity.

2.2.2. Polarization function The polarization function, Π_0, also known as charge susceptibility or non-interacting density-density response function, describes the charge fluctuation or single-particle transitions. Therefore, it is imperative to further describe collective excitations and screening in materials. For small-scale systems, such as large-angle twisted moiré structures whose eigenstates and eigenvalues can be obtained by diagonalization of the Hamiltonian, the polarization function can be solved by using the Lindhard function [116–118]

$$\Pi_0(\mathbf{q},\omega) = \frac{g_s}{(2\pi)^2}\int_{\mathrm{BZ}} d^2\mathbf{k}\sum_{l,l'}\frac{n_{\mathrm{F}}(E_{\mathbf{k}'l'}) - n_{\mathrm{F}}(E_{\mathbf{k}l})}{E_{\mathbf{k}'l'} - E_{\mathbf{k}l} - \omega - \mathrm{i}\delta} \times |\langle \mathbf{k}'l'|\mathrm{e}^{\mathrm{i}\mathbf{q}\cdot\mathbf{r}}|\mathbf{k}l\rangle|^2, \tag{6}$$

where $\mathbf{k}'$=$\mathbf{k}$+$\mathbf{q}$, $\delta \to 0^+$. Generally, the integral is taken over the whole BZ, same as in equation (1). Note here that we named the polarization function without many-body effects and local field effects as $\Pi_0(\mathbf{q},\omega)$.

Combining the TBPM with the Kubo formula, the polarization function can also be described as [105, 119]

$$\Pi_0(\mathbf{q},\omega) = -\frac{2}{\Omega}\int_0^\infty \mathrm{d}t\, e^{i\omega t}\mathrm{Im}\langle\varphi|n_F(H)e^{iHt}\rho(\mathbf{q})e^{-iHt}[1 - n_F(H)]\rho(-\mathbf{q})|\varphi\rangle, \tag{7}$$

in which $\rho(\mathbf{q}) = \sum_i c_i^\dagger c_i \exp(i\mathbf{q}\cdot\mathbf{r}_i)$ is the density operator, $\mathbf{r}_i$ is the position of the ith orbital and Ω is the area of a moiré structure system, $|\varphi\rangle$ has the same form as equation (3). Equation (7) is equivalent to the Lindhard function (equation (6)), which has been widely used in the study of single-layer graphene and twisted bilayer graphene [120]. The

Lindhard function has the advantage that it can be used to study specific attributions of band transitions, such as the intraband and interband contributions to the polarization function in moiré structures, while this information cannot be extracted from equation (7). However, when the full-band contribution to the polarization function is required to investigate screening effects in moiré structures, equation (7) will be a reliable choice with lower computational complexity in comparison to the calculation of the Lindhard funtion (6) since it includes all possible electronic excitations in moiré structures. More details related to the TBPM and equation (7) are discussed in [105].

2.2.3. Dielectric function and plasmons The dielectric function can be derived from the polarization function, $\Pi_0(\mathbf{q},\omega)$, or the optical conductivity $\sigma(\omega)$. In the random phase approximation (RPA), the dielectric function relates directly to $\Pi_0(\mathbf{q},\omega)$ as

$$\varepsilon(\mathbf{q},\omega) = 1 - V(q)\Pi_0(\mathbf{q},\omega), \tag{8}$$

where $V(q)$ is the Fourier component of the Coulomb interaction. For example, the pure two-dimensional Coulomb interaction is $V(q) = 2\pi e^2/(\varepsilon_{\mathrm{B}} q)$ with ε_{B} the background dielectric constant. Specifically, in the long wavelength limit $\mathbf{q} \to 0$, the RPA dielectric function is linked to $\sigma(\omega)$ as [121]

$$\varepsilon\left(\mathbf{q},\omega\right) = 1 + \frac{iq^2 V(q)}{\omega}\sigma\left(\omega\right). \tag{9}$$

Note that the accuracy of equation (9) is lower when q gets larger due to the local approximation used in the optical conductivity, but equation (8) is valid even for large q because the polarization function is not a local property and dependent on q, whereas the optical conductivity $\sigma(\omega)$ is independent on q. The internal electronic screening potential can be given by the dielectric function as [122]

$$V_{scr}(\mathbf{q},\omega) = \frac{V(q)}{\varepsilon(\mathbf{q},\omega)}. \tag{10}$$

A plasmon mode with momentum $\mathbf{q}$ and frequency ω_p can be obtained from the dielectric function with $\varepsilon(\mathbf{q},\omega) = 0$ [122]. The plasmon mode can be also measured from the electron energy loss function

$$S(\mathbf{q},\omega) = -\mathrm{Im}\frac{1}{\varepsilon(\mathbf{q},\omega)}, \tag{11}$$

with a sharp pole when $\omega = \omega_p$. The loss function is closely related to results obtained with EELS in experiments since the peaks in the data are related to the energy of the plasmon modes. Besides the experimental quantities of $\sigma_{\alpha\beta}(\omega)$ and $S(\mathbf{q},\omega)$ that can be directly reproduced by the numerical calculations, these optical quantities could shed light on calculated electronic structures, for example, the bandwidth, band gap and Fermi velocity and so on, which is a good starting point to further understand exotic quantum phases.

Here, it should be noted that the limitation of RPA when the charge density is small and dimension of moiré structures is low, since vertex corrections could not be safely ignored in the dielectric function calculation [123]. Based on many-body

perturbation theory, the effects of vertex corrections on the dielectric function can be evaluated by taking into account the interaction between two non-interacting Green functions [124–126], which are employed to derive the non-interacting density-density response function equation (6). Actually, previous studies have shown that vertex corrections has an impact on polarization function and plasmons in both doped and undoped graphene [125–127]. Beyond RPA, the exchange-correlation (EX) effects also play a role in affecting the dielectric function and plasmons [128]. But, the EX effects can be incorporated into the RPA scheme using local-field corrections, which could be formulated by a dielectric function with a local-field factor that cannot be determined by a self-consistent calculation [129–132].

2.2.4. Local field effects When confronted with inhomogeneous electron systems, it is crucial to consider the local field effects (LFE) [133, 134], via an umklapp process in the analysis of optical properties and plasmons [135–137]. The local field effects become stronger as the momentum transfer q increases, since then the wavelength of the excitation becomes smaller and one has to take the inhomogeneities of the electronic system under consideration. For example, for a moiré structure with large moiré length and/or large wavenumber q, when the investigated q becomes comparable to the length of the first reciprocal moiré lattice vector, the LFE could significantly change the plasmon properties. The polarization function of including the LFE is given by

$$\Pi_{\mathbf{G},\mathbf{G}'}(\mathbf{q},\omega) = \frac{g_s}{(2\pi)^2}\int_{\mathrm{BZ}} d^2\mathbf{k}\sum_{l,l'}\frac{n_{\mathrm{F}}(E_{\mathbf{k}'l'}) - n_{\mathrm{F}}(E_{\mathbf{k}l})}{E_{\mathbf{k}'l'} - E_{\mathbf{k}l} - \omega - \mathrm{i}\delta} \times\langle\mathbf{k}l|\mathrm{e}^{-\mathrm{i}(\mathbf{q}+\mathbf{G})\cdot\mathbf{r}}|\mathbf{k}'l'\rangle\langle\mathbf{k}'l'|\mathrm{e}^{\mathrm{i}(\mathbf{q}+\mathbf{G}')\cdot\mathbf{r}}|\mathbf{k}l\rangle, \tag{12}$$

where $\mathbf{G}$ and $\mathbf{G}'$ are arbitrary reciprocal lattice vectors. The dielectric function within LFE is given by the following matrix under RPA.

$$\varepsilon_{\mathbf{G},\mathbf{G}'}(\mathbf{q},\omega) = \delta_{\mathbb{G},\mathbb{G}'} - V(\mathbf{q}+\mathbf{G})\Pi_{\mathbf{G},\mathbf{G}'}(\mathbf{q},\omega), \tag{13}$$

with the two-dimensional coulomb potential $V(\mathbf{q}+\mathbf{G}) = 2\pi e^2/\varepsilon_{\mathrm{B}}(\mathbf{q}+\mathbf{G})$. The off-diagonal matrix elements in equation (13) give rise to LFE. If $G = G' = 0$, the dielectric matrix equation (13) reduces to the Lindhard dielectric function in equation (8). The optically detected macroscopic dielectric function is given by [133, 134]

$$\epsilon_M(\mathbf{q},\omega) = \frac{1}{\varepsilon^{-1}_{G=0,G'=0}(\mathbf{q},\omega)}, \tag{14}$$

where ε^{-1} is the inverse of the matrix $\varepsilon_{\mathbf{G},\mathbf{G}'}$. By comparing the macroscopic dielectric function $\epsilon_M(\mathbf{q},\omega)$ to equation (8), one can know how LFE affect optical properties in a crystal [135]. The energy loss function is formulated as $S(\mathbf{q},\omega) = -\mathrm{Im}(\frac{1}{\epsilon_M(\mathbf{q},\omega)}) = -\mathrm{Im}[\varepsilon]^{-1}_{G=0,G'=0}(\mathbf{q},\omega)$.

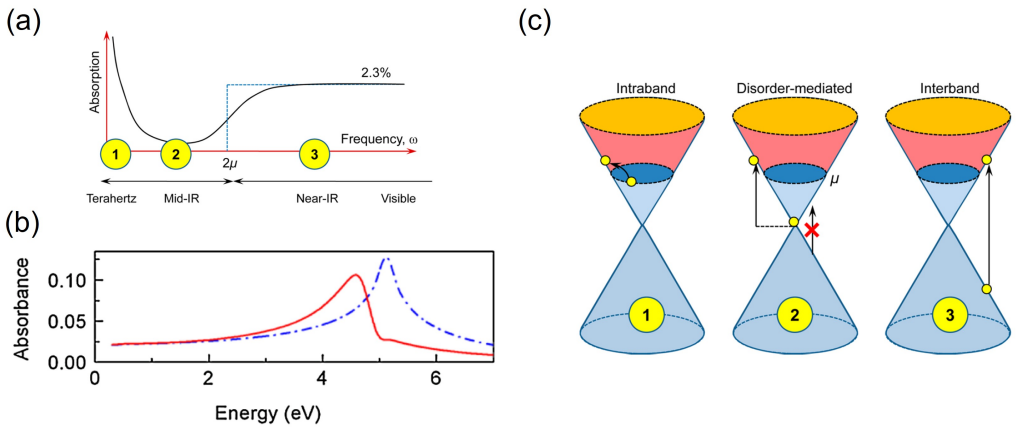


Figure 1. Optical conductivity in monolayer graphene. (a) Illustration of a typical absorption spectrum of doped graphene. Reprinted with permission from [86]. Copyright 2014 American Chemical Society. (b) First-principles absorbance of graphene with (red line) and without (blue line) excitonic effects included. Reprinted with permission from [138] Copyright (2009) by the American Physical Society. (c) Illustration of the various optical transition processes. Reprinted with permission from [86]. Copyright 2014 American Chemical Society.

3. Optical properties and plasmons in non-twisted moiré structures

3.1. Optical conductivity in graphene-based moiré structures

The optical properties of the graphene monolayer have many intriguing features [82–84], such as a constant optical conductivity in the infrared regime and gate-dependent optical absorbance [86]. As shown in Figure 1, firstly, there is a Drude peak at terahertz (THz) frequencies due to the intraband transitions. Secondly, for graphene with doping μ, a minimal absorption in the mid-infrared frequencies occurs at finite $\omega < 2\mu$ due to Pauli blocking. Thirdly, a transition occurs around $\omega \approx 2\mu$ where direct interband processes lead to a constant optical conductivity $\sigma_0 = \pi e^2/2h$. Finally, a sharp peak is located at $2t$ (with t the intralayer nearest neighbor hopping in graphene) arising from the interband transitions between the two van Hove singularities (VHS), which are logarithmically divergent points in electronic density of states (DOS) and corresponding to saddle points of band structure . This peak becomes red-shifted with a different line shape if we consider the electron-hole interaction [138].

Graphene is usually supported on top of a hBN substrate to retain a high quality. When graphene is placed on the hBN substrate, a moiré pattern of 14 nm is formed in aligned samples due to the 1.8% lattice mismatch between these two 2D materials [139–141]. Undoubtedly, the periodic moiré potential induced in the graphene-hBN structure changes significantly the electronic structure of graphene and leads to various novel quantum phenomena such as the emergence of the second-generation Dirac cones (located around some moiré energy E_M), the renormalization of the Fermi velocity, and a gap opening in the intrinsic Dirac cone [141].

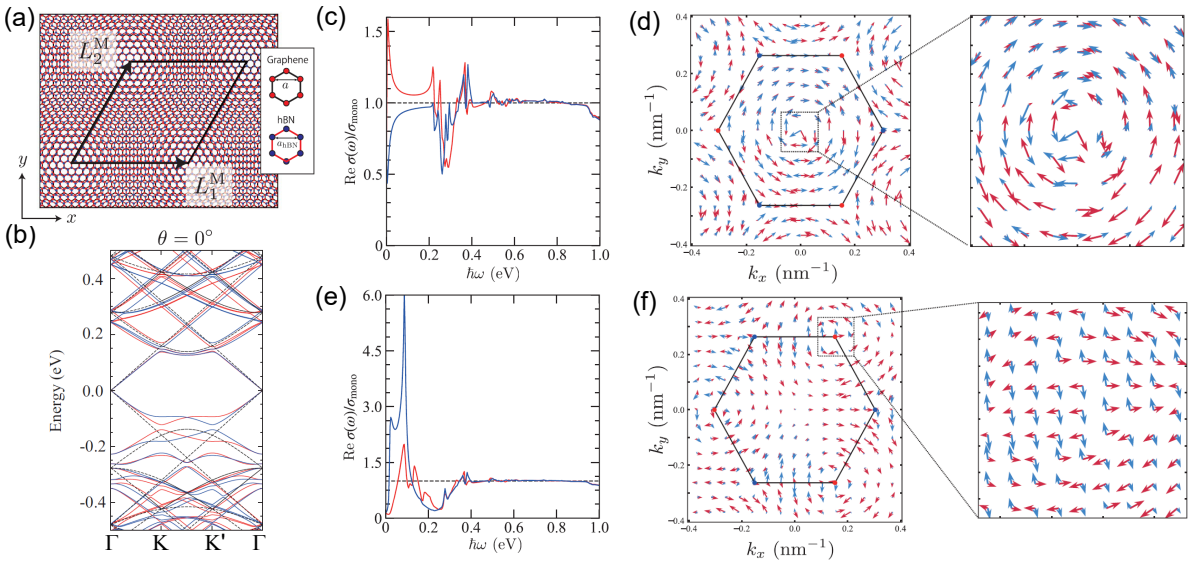


Figure 2. Valley polarization of graphene-hBN structure under circularly polarized light irradiation. (a) Crystal structure of graphene-hBN structure in real space for alignment case. (b) The band structure of graphene-hBN in the continuum model. (c) Optical conductivity of graphene-hBN for K valley and Fermi level $E_F = 0$ eV under circularly polarized light. The magenta (cyan) curve is the conductivity for LCP (RCP). (d) Distribution of dipole vectors for an interband transition near the $E_F = 0.0$ eV in momentum space. The magenta (cyan) arrows are the real (imaginary) parts of the dipole vectors. The black hexagon is the moiré BZ and the magenta (cyan) dots at the hexagon corners are the K (K') points. (e) The optical conductivity and (f) distribution of dipole vectors for $E_F = -0.13$ eV. Reprinted with permission from [144] Copyright (2022) by the American Physical Society.

In the graphene-hBN moiré structure, there is a fast sublattice oscillation due to boron and nitrogen sites which results in a series of periodic potentials acting on the graphene monolayer [142]. The first one is an scalar potential, which results from the moiré variation of the onsite terms, the second is a mass term originated from a local variation of the boron and nitrogen onsite terms, and a third one is a gauge potential resulting from the relaxation of the graphene atomic positions due to the presence of the hBN substrate [142, 143]. The resulting potential, coupled to the electron pseudospin, can be probed directly through infrared spectroscopy, because optical transitions are very sensitive to wave functions of excited states. Consequently, in the experiment in Ref. [142], a remarkable absorption peak was detected around $2E_M \sim 380$ meV, which was only observed in the graphene-hBN heterostructure. Moreover, the absorption peaks were found to be very sensitive to electron doping, which was revealed by a sharp decrease in its weight while increasing the electron concentration [142]. The sharp drop could not be explained by the single-particle Pauli blocking effect whose energy was found to be small, but was due to a renormalization of the effective potential parameters induced by electron-electron interactions.

On the other hand, it is well-known that optical conductivity is typically dominated

by the intraband Drude peak and interband transitions associated with singularities in the DOS. Theoretical works can provide a better understanding of which transitions among Bloch bands contribute to the optical conductivity. For instance, DaSilva [145] employed a $\mathbf{k}\cdot\mathbf{p}$ continuum Dirac model and the Kubo formula to investigate the optical conductivity of graphene aligned with hBN (as shown in Figure 2(a)). They discovered that the moiré pattern induced sharp THz peaks due to transitions between Bloch bands formed by the moiré potential. The particle-hole asymmetry of the moiré Bloch bands (see Figure 2(b)) was strongly reflected in the THz and IR conductivity, which was always Drude-dominated when the Fermi level lied above the Dirac point, but it was interband-dominated when the Fermi energy lies in a relatively narrow interval below the Dirac point. In addition, Abergel [146] suggested that a study of the absorption spectra as a function of the doping for an almost completely full first miniband was necessary to extract meaningful information about the moiré characteristics from optical absorption measurements as well as to distinguish between various theoretical proposals for the physically realistic interactions between graphene and hBN. One of the main findings on Ref. [146] was the fact that distinct moiré perturbations can result in similar absorption spectra.

The effect of polarized light was studied in Ref. [144]. It was found that a broken spatial symmetry in the graphene-hBN structure may induce valley polarization, which could be investigated by measuring the optical conductivity under circularly polarized light irradiation, as shown in Figures 2(c) and (e). The conductivity depended on the direction of rotation of the circularly polarized light, especially in the infrared and terahertz regions. In particular, for a photon energy ~~less~~ smaller than 0.1 eV, the difference between left-handed circularly polarized light (LCP) and right-handed circularly polarized light (RCP) became larger. In this energy region, the interband transition from valence to conduction bands dominated. The real and imaginary parts of the dipole vectors are orthogonal at the Γ point. Thus, the valley-selective circular dichroism (valley polarization) was induced by the irradiation of circularly polarized light, and was responsible for the states near the Γ point (Figure 2(d)). For hole doping case, in the region of $\omega < 0.1$ eV, the difference in the optical conductivities between LCP and RCP became larger. The real and imaginary parts of the dipole vectors are mutually orthogonal at the K and K' points, which were responsible for the valley-selective circular dichroism. In fact, the moiré potential of aligned graphene-hBN structures can be tuned by a twist angle that continuously change optical intraband and interband transitions in graphene-hBN moiré structures [147].

3.2. Plasmons in graphene-based moiré structures

The plasmons in graphene-based heterostructures [10] have attracted a lot of attentions due to the fact that plasmons in pristine graphene have very promising perspectives [148, 149]. In this section, we will mainly review plasmonic properties in graphene-hBN and graphene-metal moiré structures.

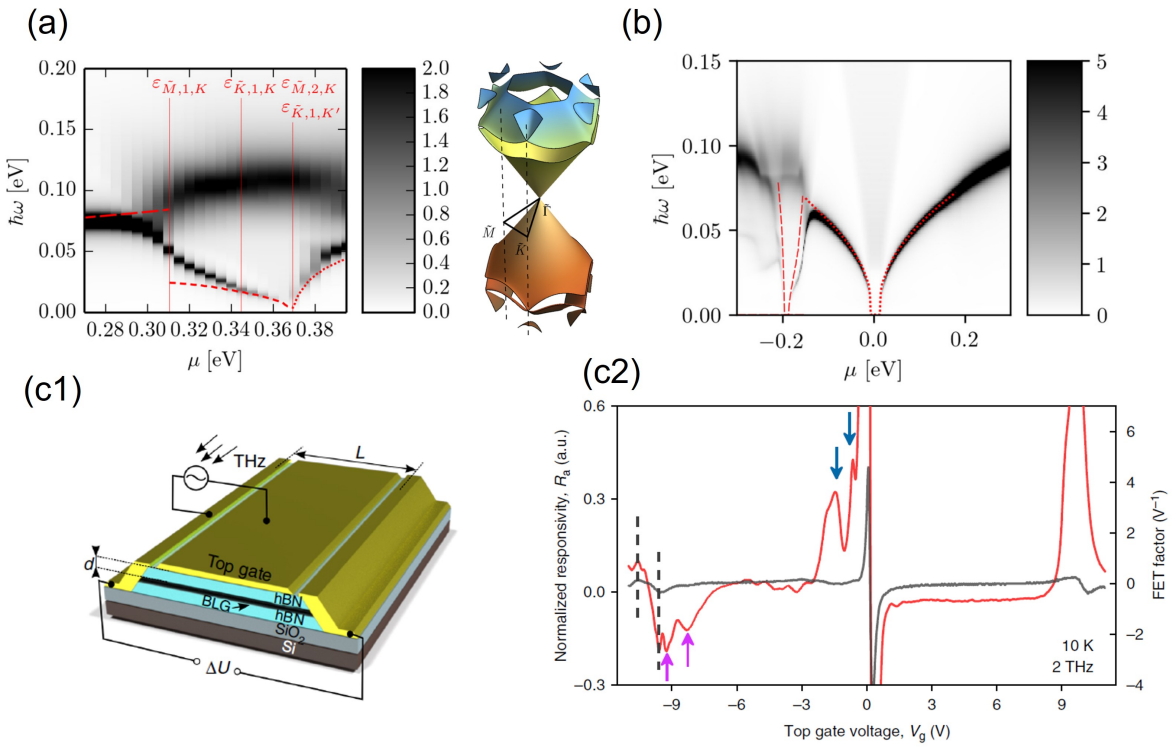


Figure 3. Plasmon in graphene-hBN moiré structures. (a) Theoretical predicted plasmon energy relation versus hole-side chemical potential in a density plot of loss function within LFE (left-hand side) and corresponding miniband structure of graphene-hBN (right-hand side). The vertical thin solid lines in the density plot denote the doping levels crossing diferent band edges in the miniband structure.Reprinted with permission from [150] Copyright (2014) by the American Physical Society. (b) Particle-hole asymmetric plasmon emerging in a density plot of loss fucntion within LFE for graphen-hBN moiré structure. Reprinted with permission from [151] Copyright (2019) by the American Physical Society. (c1) Illustration of the encapsulated bilayer graphene-hBN field effect transistor. (c2) Plasmons from miniband transition in bilayer graphene-hBN structure. Reprinted from [152] CC BY 4.0.

As mentioned in section 3.1, stacking graphene on a hBN substrate allows to engineer the electronic band structure of graphene by the induced moiré potential. An important consequence is the emergence of satellite Dirac points in the moiré minibands [153] since they could give rise to collective excitations that are different from pristine graphene. In 2014, a theoretical study on plasmons in graphene-hBN unveiled that new plasmon modes can be generated due to transitions between satellite Dirac points, as shown in Figure 3(a) [150]. The K-point and M-point plasmon modes (dotted and short-dashed lines in Figure 3(a), respectively), appeared alongside a Dirac plasmon mode (long-dashed line) in hole-doped graphene. Based on a continuum model and including the LFE, further calculations demonstrated a dramatic asymmetry of the plasmon dispersion at positive and negative potentials, as seen in Figure 3(b), and also predicted several plasmon modes arising from interband transitions between minibands. Experimentally, the measured optical response using a s-SNOM tip in

moiré-patterned graphene was enhanced with respect to pristine graphene [97]. A composite plasmon in graphene-hBN moiré structures was also observed, originating from intraband transitions near the Fermi energy and predicted interband transitions corresponding to structure mini-bands [97]. Nevertheless, up to date, the calculated terahertz plasmon from [150] and asymmetry plasmon from [151] have not been observed experimentally. In addition, based on an antenna-mediated coupling of a bilayer graphene (BLG) field-effect transistor device, shown in Figure 3(c1), miniband plasmons in BLG-hBN were also observed (see Figure 3(c2)).

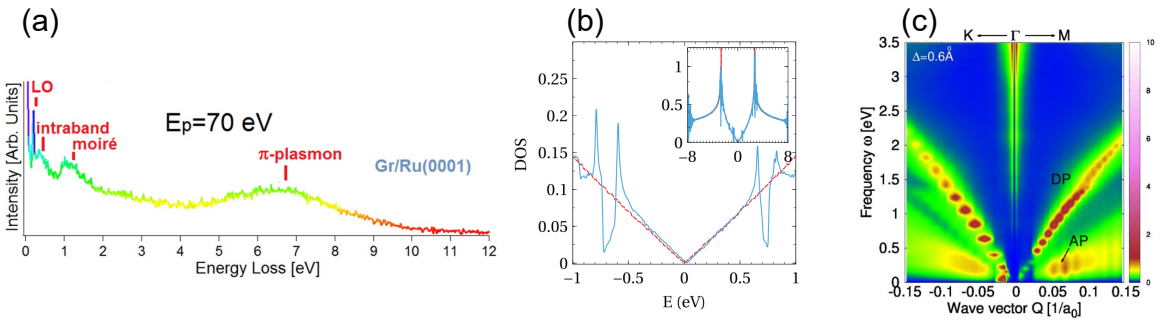


Figure 4. Plasmon in graphene-metal moiré structures. (a) High-resolution electron energy loss specstroscopy of graphene on Ru(0001), aquired with an energy of the primary electron beam E_p of 7 eV. The longitudinal optical (LO) phonon, intraband plasmon, moiré plasmon and π-plasmon are observed. (b) moiré VHS in graphene-Cu moiré structures from density functional theory calculations. Used with permission of IOP Publishing, Ltd, from [154]; permission conveyed through Copyright Clearance Center, Inc. (c) The loss function intensity plot showing an acoustic plasmon (AP) predicted in graphene-metal structure doped with alkali-metal atoms. Reproduced with permission from [155] Copyright (2019) by the American Physical Society.

The observation of miniband plasmons in graphene-hBN also motivated the exploration of electronic excitations in graphene-metal structures. The moiré potential was induced when Cu atoms were deposited on graphene, forming a moiré structure, giving rise to extra VHS associated with minibands (see Figure 4(b)). This resulted in a moiré plasmon mode with energy $\sim$ 1.5 eV, which was contributed by interband transition between VHS (as shown in Figure 4(a)). The existence of this plasmon mode was theoretically confirmed by using the TBPM method [154]. Interestingly, when the moiré potential induced in chemically doped graphene on the Ir(111) metallic surface was suppressed, plasmon could be still significantly modified, generating an acoustic plasmon (AP) mode along with an intraband Dirac plasmon (DP) mode (see figure 4(c)) [155]. This AP was induced by the screening effect of metallic materials or graphene-metal hybridization rather than by the moiré reconstruction and had also been widely studied in previous works [156–158].

4. Optical properties and plasmons in twisted moiré structures

4.1. Optical conductivity of twisted bilayer graphene

The recent discovery of correlated electronic states and superconductivity in TBG [12, 15, 51] has sparked a great interest in twisted moiré systems. In TBG the interlayer interactions induce significant distortions in the low-energy bands. This leads to distinctive electronic effects that differ from those observed in non-twisted graphene systems. At low angle, the interference between the moiré periods produces a long wavelength moiré pattern [14, 159–164]. Characteristic properties like VHS and band gaps become evident in the infrared region [115] and theoretical works [14,159–165] have demonstrated that the moiré patterns in TBG can give rise to narrow bands that largely contribute to the correlated effects observed in this system [15–17,23,24,51,62,166–179].

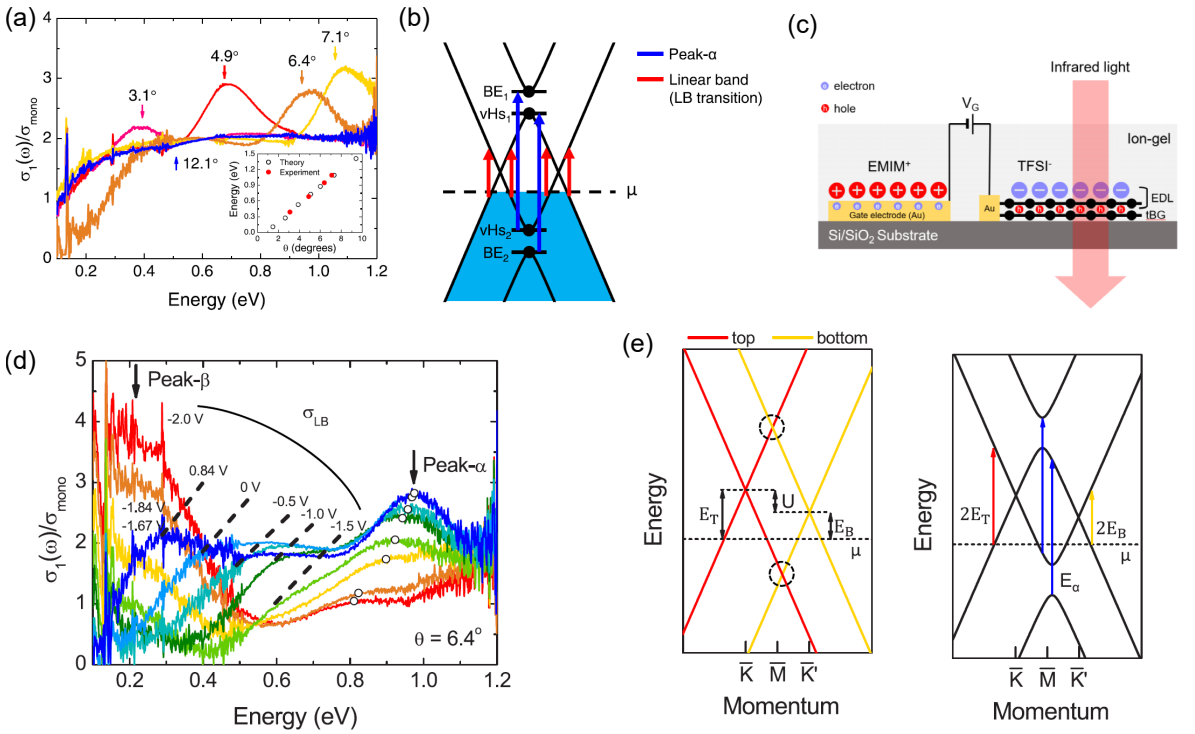


Figure 5. Gate tunable optical absorption of TBG. (a) Optical conductivity σ_1 of five TBG samples with five different twist angles. σ_{mono} is the optical conductivity of monolayer graphene. (b) Electronic band diagram of TBG. BE and vHs stand for the band edge of the second band and the saddle-point van Hove singularity, respectively. There exist two kinds of optical transitions as indicated by the red and blue arrows. (c) Schematic view of the ion-gel gating circuit and the infrared transmission measurement. EMIM and TFSI are ionic liquids. (d) Optical conductivity of TBG with various gate voltages V_G. The twist angle is $\theta = 6.4°$. (e) (Left side) The band structure of TBG under gating. The top band and bottom band shift by E_T and E_B, respectively. $U = E_T - E_B$ is their difference. Here, the gap opening is omitted for clarity. (Right side) Optical transitions of the gated TBG. Reprinted with permission from [180] Copyright (2019) by the American Physical Society.

An interesting feature of TBG is that the VHS can be moved to arbitrarily low energies by modifying the twist angle. One interesting optical analysis of TBG was performed by Yu *et. al.* [180]. In the experiment, different optical conductivities were obtained by varying the twist angle. As shown in Figure 5(b), the low-energy optical spectrum of TBG was characterized by a linear-band (LB) absorption (pointed out by the red arrows). This was an indication that the interlayer interaction hybridized the LBs of the two monolayers and, as a consequence, there were two isolated bands with an avoided crossing with the remote bands. In Figure 5(b), the transition between the saddle-point $VHS_2 \rightarrow VHS_1$ was forbidden by the lattice symmetry [115]. However, the transition between VHS and the band edge (BE) of the second band exhibited prominent peaks (peak-α indicated by the blue arrows). Two interesting features, shown in Figure 5(a), were found in this experiment: firstly, a frequency-independent conductivity, $2\sigma_0$, which came from the LB transition, and secondly, an angle-dependent peak-α resulting from the transitions between VHSs and BE. Interestingly, the peak-α was blueshifted as the twist angle θ increased, revealing a dependence on the twist angle. Furthermore, by designing an ion-gel gating circuit (in Figure 5(c)) it was possible to investigate the gating effect on the properties of these devices. It was found that in the absorption profile, cf. Figure 5(d), (i) the absorption edge of σ_{LB} had a broadening and was shifted to higher energy, and (ii) the peak-α was shifted to a lower energy with a reduced intensity. In addition, a modification of the band structure with gating was found, because in the presence of a vertical electric field, Figure 5(e), the Dirac cones of each monolayer shifted in opposite directions. This was theoretically described in [181] and recently in [182], allowing to modify the optical transitions [183].

Additional evidence of the existence of isolated narrow bands with an enhanced density of states was reported in 2013 by Zou et al. [184]. By means of a terahertz time-domain spectroscopy, the optical conductivity of TBG was obtained at different temperatures in the frequency range 0.3–3 THz. One of the main findings in this work was a Drude-like response with a strong peak in $\sigma_1(\omega)$ at ~ 2.7 THz, which was identified as peak-α in TBG with $\theta = 1.16°$.

Interestingly, TBG shows an angle-dependent optical conductivity, which could be utilized to characterize the twist angle. For example, Sunku et al. [93] combined nano-photocurrent and infrared nanoscopy methods, which enabled access to the local electronic phenomena at length scales as short as 20 nm, and identified domains of varying local twist angles. In addition, Calderón [185] reported that the optical conductivity measurements could be used to distinguish different symmetry breaking states, and may reveal the nature of the correlated states in the flat bands that appear in TBG. As shown in Figures 6(a)-(c), in a correlated order which breaks the $\mathcal{C}_2\mathcal{T}$ symmetry, named α here, a gap was opened at the Dirac points in K, resulting in a reorganization of the spectral weight. In TBG without correlations or external symmetry breaking, the lattice had $\mathcal{C}_3$ symmetry, Figure 6(f). Moreover, in a system with $\mathcal{C}_3$ symmetry$\sigma_{X_iX_j} = \sigma_{Y_iY_j}$. Here, X_i is the direction, as illustrated in Figure 6(f). Therefore, the optical conductivity along the four directions (X_1X_1, X_2X_2, Y_1Y_1

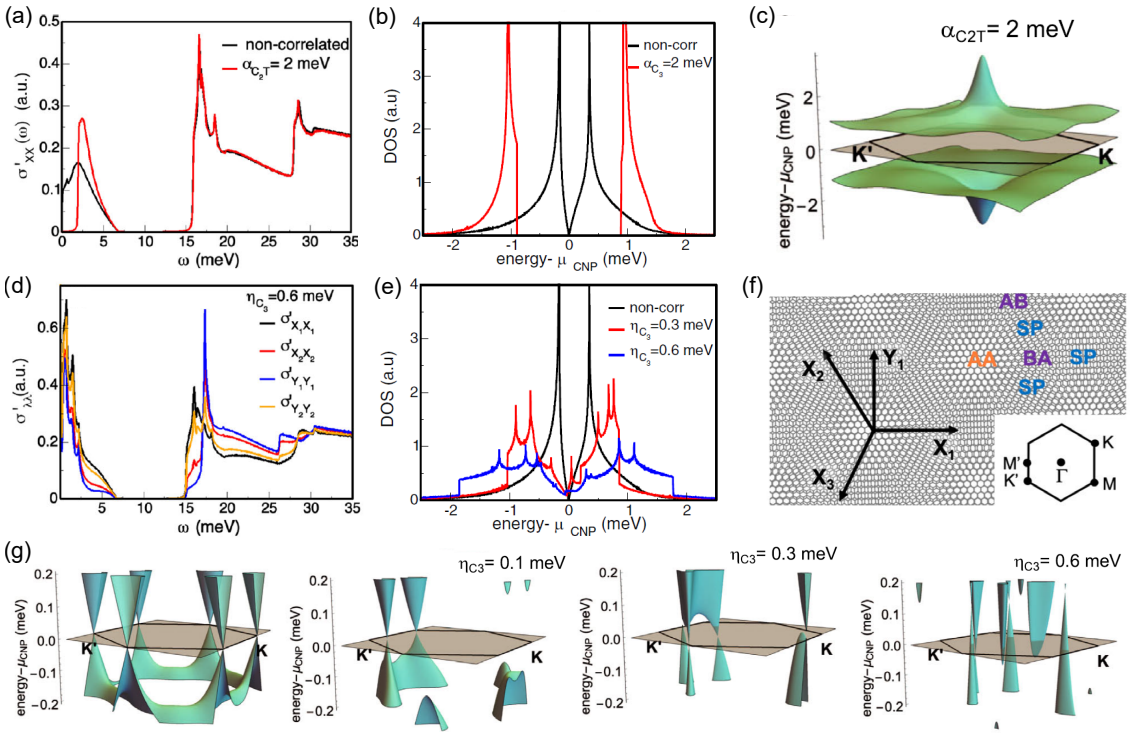


Figure 6. Optical conductivity, DOS and band structures of undoped TBG with different symmetry breaking orders. (a) Optical conductivity, and (b) low energy DOS of the TBG at the CNP in a C_2T symmetry breaking state α and in the non-correlated state. (c) Flat bands of the TBG in the C_2T symmetry breaking state. (d) Optical conductivity and (e) DOS for the nematic state η. The optical conductivity in (d) is plotted along four different directions, illustrated in (f). (f) Sketch of the C_3 related X_i directions and of Y_1, and the BZ of TBG with the corresponding symmetry points. (g) Zoom of the flat band structure for the TBG with different values of η_{C_3}. Note that the optical conductivity in (a) along the four directions are equal. Reprinted from [185] CC BY 4.0.

and Y_2Y_2) were equal in the correlated order, but different in the reported nematic state (named η_{C_3}, which lowers the rotational symmetry of TBG). Furthermore, in the nematic state, when the flat band was partially filled, the DOS was modified. With larger values of the amplitude of the order parameter η_{C_3}, the Dirac points moved away from the charge neutrality point and hole and electron Fermi pockets were generated. Additional Fermi pockets appeared, leading to new band crossings between the lower and upper flat bands (Figure 6(g)).

On the theoretical side, we highlight the following works: in Ref. [186], the authors used a continuum model to study the frequency-dependent conductivity at different levels of chemical potential. Moon et al. [115] performed both tight-binding and continuum calculations of the optical conductivity, and analytically explained the optical selection rules in terms of the symmetry of the effective Hamiltonian. In addition, Stauber et al. [121] calculated chemical potential dependent Drude weight of the optical conductivity in TBG by means of a continuum model. The excitonic effects, for instance,

electron-hole interactions [187], and the self-consistent Hartree potential [188], were also investigated in the optical spectra of TBG. It was found that in TBG under strain [189], the peaks associated with transitions between the flat bands in the optical conductivity were highly sensitive to the direction of the strain. The effects of a magnetic field [190] and magnetic impurities on the optical conductivity [191], as well as optical activity in TBG have also been analysed [192]. Analysis in stacking configurations [193, 194], quantum dots and large twist angles ($\theta \geq 5°$) [195] reveals additional optical properties.

4.2. Optical properties of other twisted 2D materials

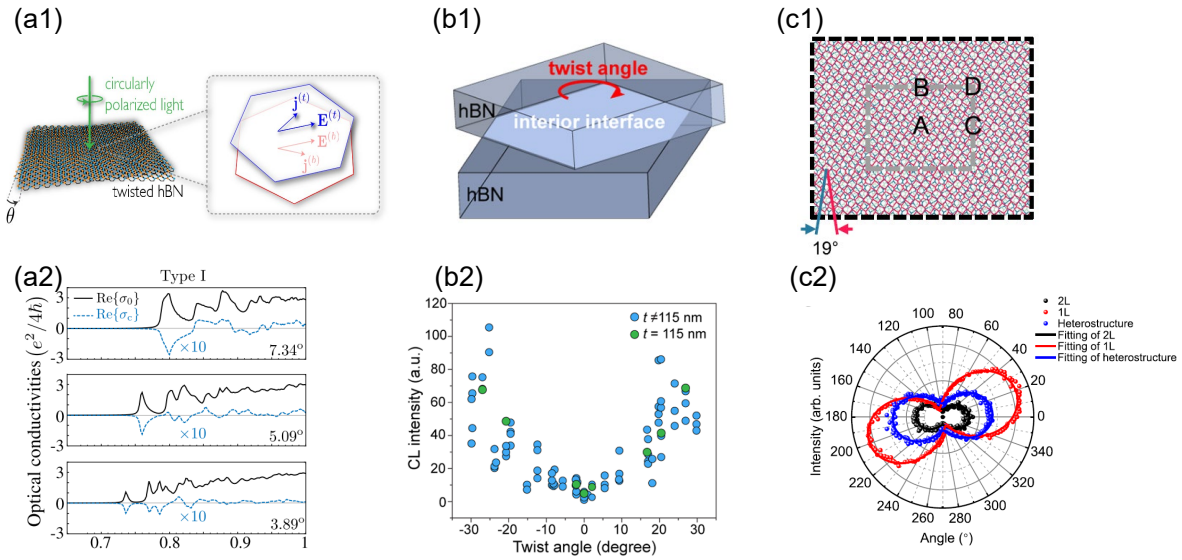


Figure 7. Optical properties of other twisted 2D materials. (a1) Illustration of twisted bilayer hBN with incident circularly light. (a2) Real part of total (black lines) and chiral (blue lines) optical conductivity. Reprinted with permission from [196] Copyright (2020) by the American Physical Society. (b2) Twist-angle dependent cathodoluminescence (CL) intensity in (b1) twisted hBN multilayers. Reprinted with permission from [197] Copyright 2021 American Chemical Society. (c2) Anisotropic photoluminescence emissions in (c1) twisted monolayer/bilayer phosphorene heterostructure with twist angle 19° comparing to monolayer (1L) and bilayer phosphorence (2L). Reprinted with permission from [198].

Owing to the chiral symmetry, twisted bilayer hBN displays circular dichroism, which has a different absorption of left and right circularly polarized light [199]. This property can be tuned by stacking and twisting [196]. The circular dichroism is proportional to the ratio of chiral conductivity to the total conductivity σ_0 (shown in Figure 7(a2)). The chiral response indicated that twisted bilayer hBN had different absorption to left and right-polarized light. Besides twisted bilayer hBN, twisted hBN films have also attracted recent experimental research, in particular Lee *et al.* [197] found that both wavelength and intensity of luminescence were tunable. These properties were found to be enhanced with the twist angle between the hBN interface layers increased,

as seen in Figure 7(b2). The origin of this enhancement was that the moiré sub-band gap decreased with twist angle. This experiment indicates that the moiré potential is relevant in the moiré structures composed of bulk-like materials .

On the other hand, moiré optical properties in twisted semiconductors have also been investigated. For example, in the anisotropic twisted monolayer/bilayer phosphorene heterostructure, shown in Figure 7(c1). The detected anisotropic optical transitions were notably different from the optical features of the corresponding monolayer and multilayer phosphorene [200, 201], even at a large angle like 19°, as illustrated in Figure 7(c2). The reason behind this effect is that the moiré potential resulted in a strong hybridization between the twisted layers. Furthermore, the optical moiré transitions were sensitive to the twist angle [198]. Additionally, the twisted heterostructure of anisotropic materials such as black phosphorus and orthorhombic molybdenum trioxide can be used to control light polarization state [202]. Twisting large angles such as $\theta = 21.81°$ and $\theta = 32.22°$ can also serve as a way to reduce interlayer interaction of bilayer MoS_2, which can induce a higher value of absortance than untwisted case [203].

4.3. Plasmons of twisted bilayer graphene

Twisted bilayer graphene offers new degrees of freedom on tuning the electromagnetic response, for example, the twist angle [187, 207, 208]. Plasmons are collective charge oscillations that lead to nanoscale optical fields. One of the pioneer works was that of Stauber *et al.* [121] who theoretically investigated the plasmonic spectrum of TBG via a continuum model. They found that the TBG interlayer coupling gave rise to a finite Drude weight, even in the undoped case. This allowed for the existence of plasmons that was weakly Landau-damped due to the quasi-localized nature of the interband transition states. As shown in Figure 8(b), acoustic interband plasmon modes appeared at zero chemical potential and changed to conventional $\sqrt{q}$ modes with non-zero doping levels in the first magic-angle (1.05°) TBG [121]. Moreover, plasmon modes in TBG were dependent on both twist angle and the chemical potential. Interestingly, quasi-flat plasmon modes and renormalized Fermi velocity (approached zero) were predicted in TBG even for twist angles ($\sim 1.61°$) larger than the magic angle, as seen in Figure 8(c). These collective excitations were explained as oscillation of localized states around the AA regions (see Figure 8(a)) [204]. Moreover, intrinsically undamped and quasi-flat plasmon modes were discovered in doped magic-angle graphene, as depicted in Figure 8(d) [205]. Conversely, at zero doping, including the effects of atomic relaxation, low-damped and damped plasmons were observed to emerge in the magic-angle configuration [120]. A further theoretical study found that in the long wavelength limit, the plasmon energy could be independent of doping level, but can be tuned by the bias voltage in magic-angle TBG [209]. These findings distinguish the TBG system from the 2D electron gas (2DEG) that has a traditional $\sqrt{q}$ plasmon dispersion with energy dependent on charge density [210]. Moreover, other unusual plasmon features such as plasmonic Dirac

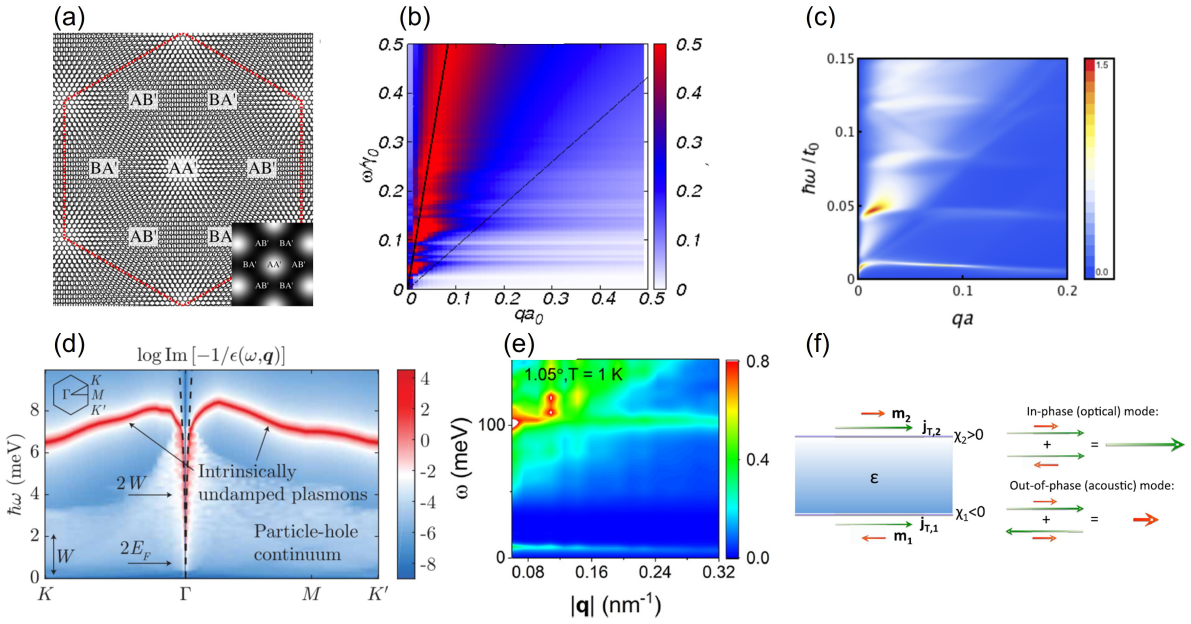


Figure 8. Theoretical exploration of plasmons in twisted bilayer graphene. (a) Moiré structure of twisted bilayer graphene. The moiré pattern contains AA, AB and BA high-symmetry stackings. (b) Linear plasmon emerging in the loss function intensity plot of magic-angle twisted bilayer graphene. Reprinted from [121]. (c) Density plot of the loss function showing quasi-flat plasmons in twisted bilayer graphene at 1.61° Reprinted with permission from [204] Copyright 2016 American Chemical Society. (d) Undamped plasmons in doped magic-angle twisted bilayer graphene. W is the width of the narrow bands. E_F is the Fermi energy. Reprinted from [205]. (e) Dispersion-less and low-damped plasmon appearing in the loss function spectrum of undoped magic-angle TBG at temperature T = 1K. Reprinted with permission from [120] Copyright (2021) by the American Physical Society. (f) Chiral plasmon response in twisted bilayer graphene. Reprinted with permission from [206] Copyright (2018) by the American Physical Society.

cone and plasmon non-reciprocity, were discovered in biased magic-angle TBG [211–214]. In addition, a further design of a TBG device as in Figure 8(f), allowed to excite chiral longitudinal plasmonic modes with different phases. Additional chiral responses and plasmon edge states were exploited and were found to enhance the electromagnetic near-fields chirality in TBG [215–217]. Furthermore, theoretical studies explored how plasmon in TBG were influenced by electron-electron interaction [188, 218], finite size of TBG [219], and magnetic field [220].

Experimentally, the plasmon wavelength and damping rate were investigated by infrared s-SNOM with an excitation energy of 0.11 eV [221]. It was found that TBG with decreased twist angles leaded to the decrease of the plasmon wavelength, shown in Figure 9(b), reflecting a renormalization of the Fermi velocity of the Dirac fermions at different twist angles. A reduced Fermi velocity is attributed to the enhanced interlayer interaction at twist angles, giving rise to a relaxation of the plasmon wavelength. However, the plasmon damping rate was found to be smaller with larger twist angles,

as seen in Figure 9(c), likely due to stronger charge scattering rates [221]. On the other hand, the propagation of plasmon polaritons was studied by infrared nano-imaging in TBG [101]. A linear-like plasmon mode (that is, the dispersion of a plasmon mode is closely linear) of 1.35° TBG was observed by Hesp *et al.* [98]. The plasmon mode had an energy around 220 meV, due to interband collective excitations whose spectrum was reproduced with a continuum model with reduced AA tunnel coupling.

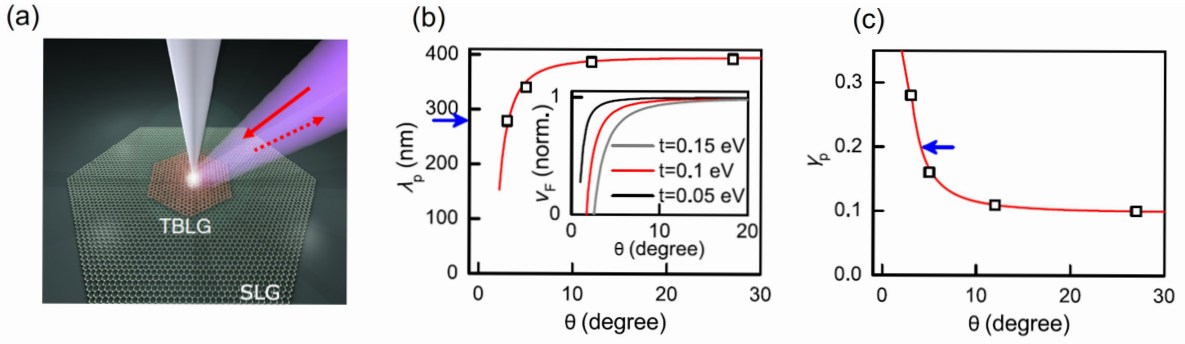


Figure 9. Experimental investigation of plasmons in twisted bilayer graphene. (a) Illustration of the nanoinfrared imaging experiment using s-SNOM in TBG using laser energy of E=0.11 eV. (b) Plasmon wavelength of TBG versus twist angles. The insets plots the normalized Fermi velocity of TBG at different interlayer coupling energy t. (c) plasmon damping rate at different twist angles. The blue arrows in (b) and (c) mark the value of plasmon wavelength and damping rate in single layer graphene, respectively. Reprinted with permission from [221]. Copyright (2017) by the American Physical Society.

In addition, chiral plasmons, the surface electromagnetic waves showing non-reciprocal propagation, in TBG were experimentally reported in Ref. [222]. They are achieved due to the uncompensated Berry flux of the electron gas under optical pumping. They were found to be characterized by two peaks appearing in the extinction spectra. These low-energy plasmon modes arose from interband transition with broken time-reversal and inversion symmetry. In the experiment, a plasmonic mode whose group velocity approaching to zero (termed slow plasmon modes) was identified around 0.4 eV, which stemmed from interband transition between subbands in lattice-relaxed AB domains [222], compared to theoretically predicted quasi-flat plasmon mode generated in the AA regions [204]. These slow plasmon modes could couple to light and form slow surface plasmon polaritons, which also provide potential for constructing optical metamaterials [223].

4.4. Plasmons of twisted multilayer graphene

Flat band and Dirac bands are found to coexist in twisted trilayer graphene with mirror symmetry [51,54]. This coexistence may allow the plasmons to have different properties from those in TBG. Theoretically, Wu *et al.* [224] numerically investigated plasmons in twisted trilayer graphene with different twist angles and vertical pressures. In particular,

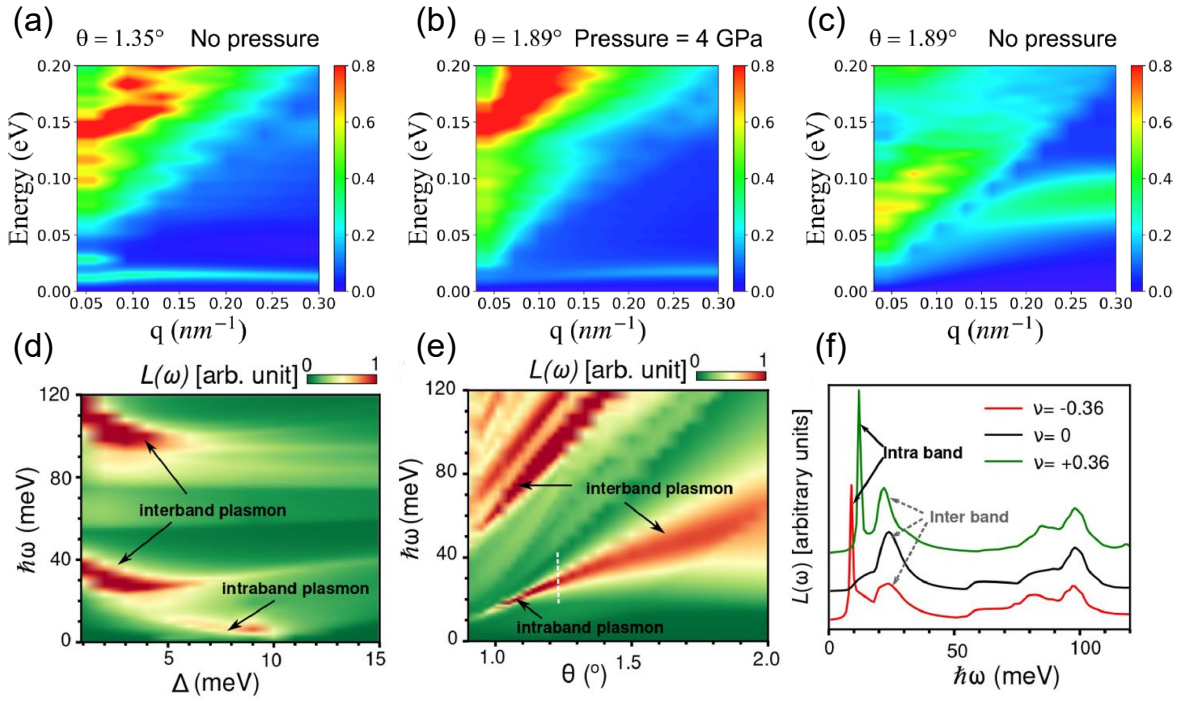


Figure 10. (a) Loss function intensity plots in the magic-angle 1.35° twisted trilayer graphene; (b) and (c) pressure engineering plasmon modes in 1.89° twisted trilayer graphene. Reprinted with permission from [224] Copyright (2021) by the American Physical Society. Twisted double bilayer graphene intraband and interband plasmons as a function of: (d) electric bias, (e) twist angle, and (f) doping level. Reprinted with permission from [225] Copyright (2022) by the American Physical Society.

for a twist angle of 1.35°, the defined magic angle at which Fermi velocity is zero in this system, a clear quasi-flat plasmon mode emerged below 0.05 eV, as seen in Figure 10(a). This plasmon was found to be originated from collective excitations inside the flat bands. As shown in Figure 10(c), for large twist angles and no pressure, the quasi-flat plasmon mode had a blue shift to an energy of 0.06 eV indicating the presence of wider bands near charge neutrality. By applying a vertical pressure, the plasmon mode reappeared, indicating an enhancement of the interlayer coupling with pressure.

On the other hand, numerical studies found that long lived, flat intraband and interband plasmons can exist in twisted double bilayer graphene [225]. In particular, it was found that a flat intraband plasmon modes emerged at long momentum because of the influence of higher interband transitions. Furthermore, as shown in Figure 10(d)-(f) these plasmon modes were found to be tuned by a vertical electric field, twist angle and doping, respectively. Gapped interband plasmon and intraband plasmon appeared at small and large electric field, respectively, and they persisted over a wide range of twist angles.

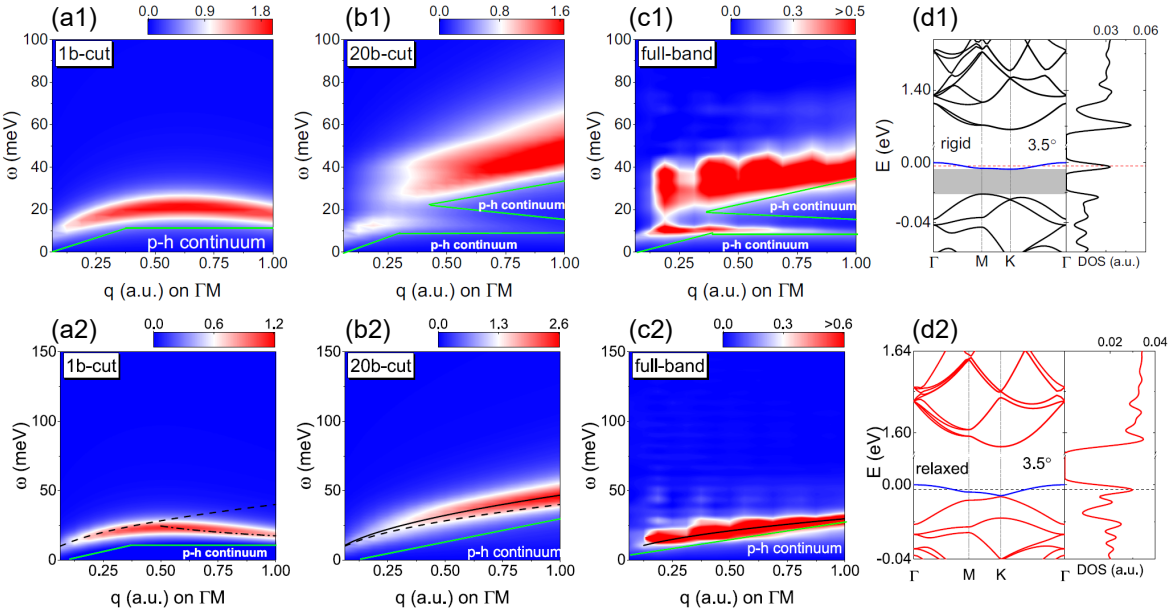


Figure 11. Loss function intensity plots of twisted bilayer MoS_2 with (first row) and without (second row) atomic relaxation. (a) Only one band, the flat band included in equation (6), while (b) 40 band near the flat band included and (c) full band of tight-binding model with TBPM as equation (7). Particle-hole (p-h) continuum region is marked with "p-h continuum" and boundaries with green solid lines. (d) The band structure of 3.5° twisted bilayer MoS_2 without lattice relaxation (d1) and within (d2). Reprinted with permission from [226] Copyright (2022) by the American Physical Society.

4.5. Plasmons of twisted bilayer transition metal dichalcogenides

In moiré TMDCs, the existence of flat bands also provides possibility to explore quasi-flat plasmon modes. A recent numerical study [226] suggested that both atomic relaxation and high energy bands have an impact on the low energy flat-band plasmon in twisted bilayer MoS_2, shown in Figure 11. In particular, for an unrelaxed system, shown in Figures 11(b1) and (c1), a flat intraband and linear interband plasmon modes were found. The distinct results between the different approximations suggested that the interband transitions play an important role in the unrelaxed system. However, the relaxation effects transformed the two plasmon modes to one mode with $\sqrt{q}$ dispersion as seen in Figure 11(b1) and (c2). Further analysis concluded that the isolation of the flat band shown in Figure 11(d1) was the key to obtain quasi-flat plasmon modes in twisted bilayer TMDCs, and the high-energy interband transitions had impact on plasmons at a large momentum limit [226]. In addition to the twist angle effect on plasmons in twisted bilayer MoS_2, a recent experiment also showed that film thickness ratio of bilayers could manipulate plasmon topology in twisted WTe_2 films [227]. Single-layer MoS_2 could provide multi-component plasmons since it features spin and valley as two extra degree of freedom [228], which could be used to engineer the plasmon properties in twisted bilayer TMDCs in future studies.

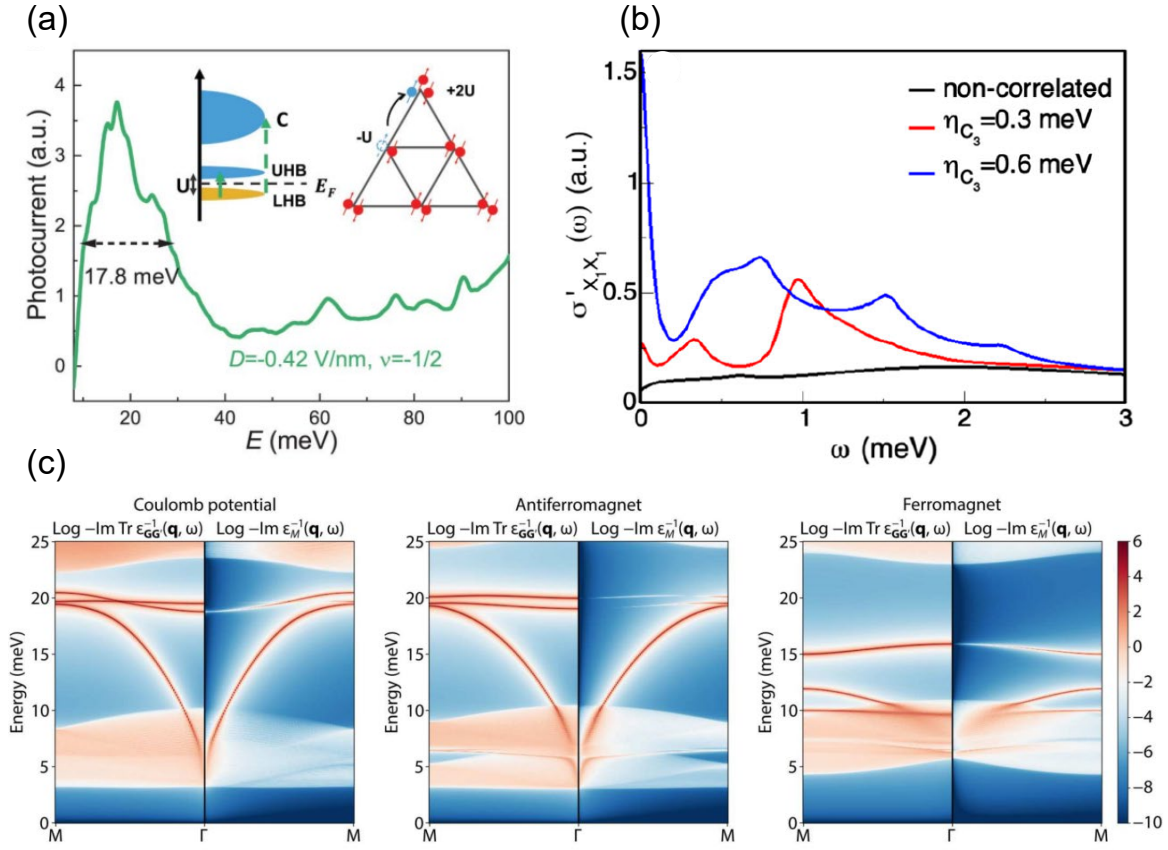


Figure 12. Many-body effects. (a) Observed optical response peak in correlated ABC trilayer graphene-hBN moiré structure [229]. The photocurrent peak corresponds to the optical transition crossing the Mott gap between lower Hubbard band (LHB) and upper Hubbard band (UHB), as illustrated by the solid arrow in the left inset.The Reprinted with permission from AAAS. (b) Optical conductivity in TBG with correlated effect (nematic order, red and blue lines) and without correlated effect (black line). η_{C_3} is the magnitude of the nematic order. Reprinted from [185] CC BY 4.0. (c) Plasmon spectrum of TBG within different many-body effect. Reprinted from [230] CC BY 4.0.

5. Relation with other properties

5.1. Many-body effects

Many-body effects can provide a significant effect on optical properties and plasmons of moiré structures. For example, optical spectroscopy was employed to probe correlations in ABC rhombohedral trilayer graphene with hBN (ABC-hBN) [229]. In this work, an optical absorption peak emerged at $\sim$ 18 meV, indicating a direct optical excitation across an emerging Mott insulator, as shown in Figure 12(a). A similar optical spectra was observed at different fillings. The optical response was found to be a useful tool to characterize the onsite Coulomb repulsion energy, U, in the corresponding Hubbard model. On the other hand, optical conductivity was also theoretically used to reveal the nature of correlated states in TBG [185]. Comparing to the optical excitation that

a Drude peak emerged at charge neutrality in non-correlated models, new absorption peaks appeared in the optical spectrum for different values of correlated nematic order parameters η_{C_3}, see Figure 12(b). Additional calculations in the same system showed that the optical conductivity can be used to distinguish different symmetry broken states. The plasmons can also be used to probe many body effects as discussed in section 4.1. Recently, Papaj *et al.* [230] proposed to probe correlated states with plasmons in twisted heterobilayer TMDCs, where a folded plasmon spectrum can be a signature of correlated states, as shown in Figure 12(c). Here, the plasmon spectra has different characteristics depending on the type of correlated effects.

5.2. Non-linear optical response

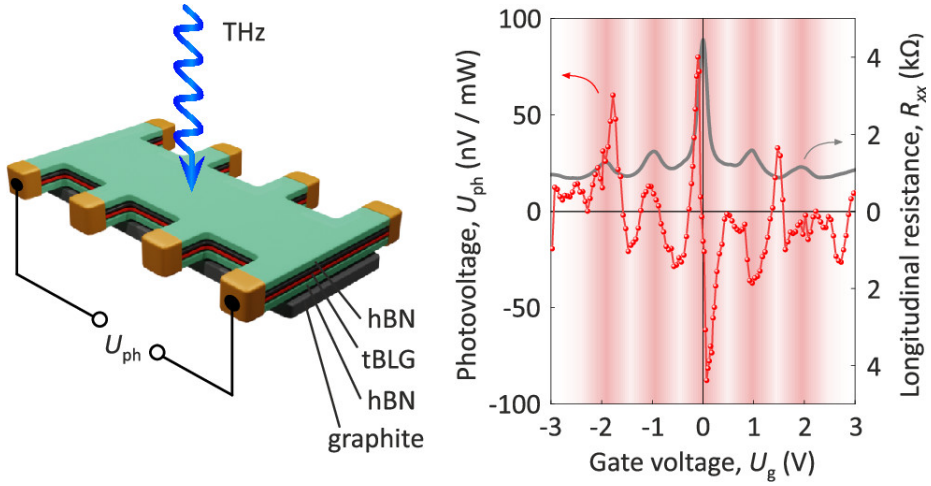


Figure 13. Photogalvanic effect in low angle TBG ($\theta = 0.6°$). (Left side) Schematics of a TBG sample encapsulated by hBN. (Right side) An incident terahertz radiation gives rise to a photovoltage. Reprinted with the permission from [231]. Copyright 2020 American Chemical Society.

The nonlinear optical response in TBG, also referred to as optotwistronics [232] or twistoptics [233], has attracted attention only recently. Theoretical works have explored the impact of light on the TBG band structure. In particular, a Floquet band engineering has been investigated by means of tight-binding models [234,235]. Due to the extensive number of sites in the TBG moiré unit cell, the continuum model has proven to be highly valuable for studying optically induced flat bands [236], the manipulation of interlayer couplings [237], and the formulation of effective Floquet Hamiltonians [238].

As mentioned in the previous section, the TBG transition energies are notably influenced by the twist angle [239, 240]. Consequently, for a constant twist angle, the activation or deactivation of one- and two-photon resonances can be achieved by adjusting the incident wavelength. This characteristic allows for a highly adaptable second harmonic generation in TBG [241, 242]. Remarkably, at larger twist angles ($\sim 21.79°$) and in the presence of intense laser fields, TBG has been found to display

high-harmonic generation, that by symmetry grounds cannot occur in monolayer or bilayer graphene [232, 243]. The selection rules described in [232] under circularly polarized light stem from the underlying lattice symmetry of TBG at large angles.

On the other hand, at low twist angles ($\sim 1.05°$) there is an interplay between twist, band geometry and optical response [243]. There is an emergence of dynamical symmetries coupled with the standard symmetries of the TBG lattice ($\mathcal{C}_{2y}$ and $\mathcal{C}_3$) which are not present at large twist angles ($\sim 21.79°$) . Additional selection rules for the current response are obtained at the low angle regime. In particular, an induced inversion symmetry breaking [244] in the bilayer system allows for a non-zero finite Berry curvature which enhances the non-linearity. Interestingly, as described in Ref. [243] the high order harmonics were found strongly dependent on the magnitude of the band geometry through the Berry curvature. The photogalvanic effect, which is the lowest order non-linear effect, was predicted [231, 245] and then experimentally observed in low-angle ($\sim 0.6°$) samples of TBG [231], see Figure 13. At higher orders, a third order optical non-linearity was also reported [246], where the non-linear response was found to be considerably modified depending on the rotation angle in TBG. Effects of the band topology [247], high harmonic generation [248], correlated insulating states [249] have also been investigated. In addtition to TBG, non-linear optical response can be achieved in large-angle ($\sim 50°$) twisted multilayer WS_2 [250]. It is worthy to mention that via a second harmonic generation in heterostructures of graphene-hBN a transtion from a commensurate to a non-commensurate state was detected [251].

5.3. Superconductivity

The origin of superconductivity in moiré twisted graphene layers remains a subject of debate [12, 257]. In addition to the proposed phonon-mediated theory [258, 259], purely electronic mechanisms such as the Kohn-Luttinger (KL) mechanism and plasmon-mediated superconductivity have also been examined [253, 255, 256]. This is motivated by the significant influence of electron-electron interactions found in magic-angle TBG [15, 18]. For instance, theoretical studies of the dielectric function within the RPA, cf. equation (10), reveal that the screened Coulomb potential calculated near the magic-angle TBG displays attractive regions in real space [253, 254, 260], see Figure 14(a), indicating that superconductivity could be induced by pure electron-electron interactions [261, 262] through a KL mechanism [253, 263]. The RPA calculations with frequency-independent polarization function show that the superconducting instability can appear near VHS and precedes a spin-density-wave instability under KL mechanism, as shown in Figure 14(b). Furthermore, the critical temperature has also been predicted based on the KL mechanism by calculating the static screened dielectric function and the gap equation [262]. However, it is worth noting that the predicted critical temperature is not as high as what has been observed in experiments, as indicated by the gray dots in Figure 14(c). This suggests that phonons may also contribute to the enhancement of the superconducting pairing [254].

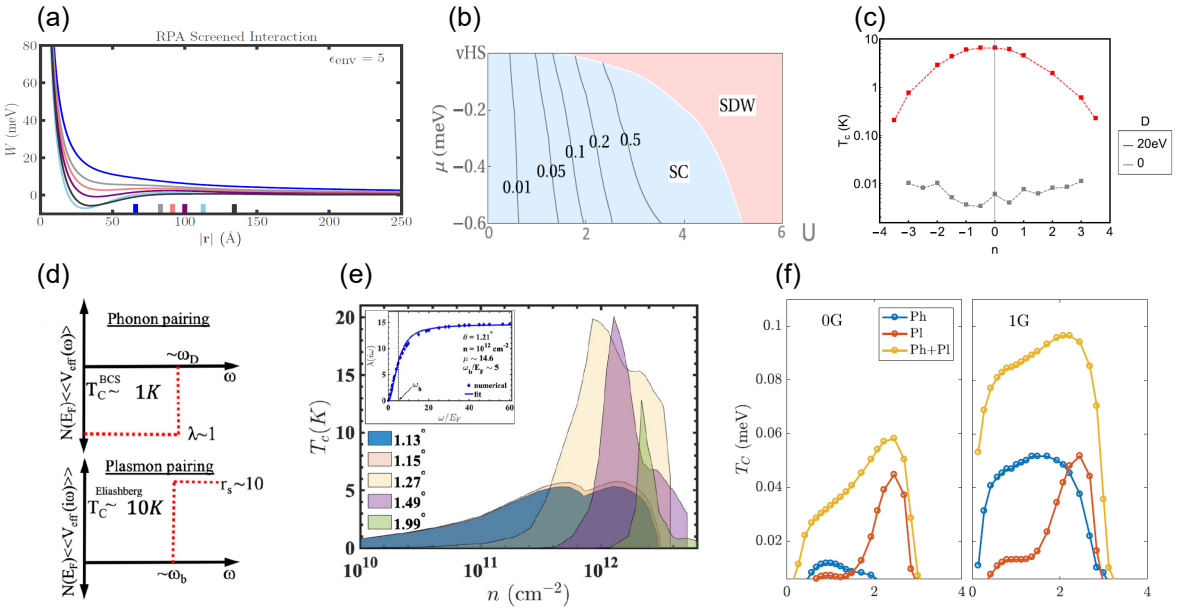


Figure 14. (a) Attractive electron-electron interaction in magic-angle twisted bilayer graphene. Reprinted with permission from [252] Copyright (2019) by the American Physical Society. (b) Purely electron-electron induced superconductor phase in magic-angle twisted bilayer graphene. Reprinted with permission from [253] Copyright (2019) by the American Physical Society. (c) Superconductivity critical temperature explained by electron-electron screening potential with (red dots) and without phonon effect (gray dots) Reprinted from [254] CC BY-NC-ND 4.0. (d) Plasmon paring driven by dynamic Coulomb interaction comparing to Phonon paring and (e) critical temperature of plasmon-mediated superconductivity in TBG at different angles. Reprinted from [255] CC BY 4.0. (f) Phonon (Ph) and plasmon (Pl) mediated superconductivity in magic-angle TBG without (0G) and within (1G) local field effect. Reprinted with permission from [256] Copyright (2021) by the American Physical Society.

On the other hand, as depicted in Figure 14(d), the intrinsic plasmon mode in magic-angle TBG is estimated to lead to an even higher critical temperature (T_c) than the effects of phonons under a massless Dirac model. Further numerical calculations reveal that the dynamical Coulomb-driven T_c can reach approximately 15 K and varies with the electron density of TBG near the magic angle, as shown in Figure 14(e). Further research delves into how the local field effect (LFE) plays a role in cooperative effects between plasmons and phonons on superconductivity [256]. As illustrated in Figure 14(f), plasmon-mediated superconductivity appears to be insensitive to LFE, which aligns with previous findings indicating that plasmons in TBG are not significantly affected by LFE [204, 205]. Recently, extrinsic screening effects on superconductivity were investigated in TBG as well, showing that the critical temperature was unaffected by screening unless the screening layer was lower than three nanometers from the superconductor [264]. Besides LFE, effect of vertex corrections on plasmon-mediated superconductivity in moiré structures could deserve some attentions

[265], while vertex corrections could be safely dropped in conventional high-density superconductors according to Migdal's theorem [266, 267]

6. Summary and Outlook

This paper reviews recent theoretical and experimental research on optical properties and plasmons in widespread non-twisted and twisted moiré structures. For non-twisted moiré graphene-based structures, the moiré potential plays a key role in producing saddle points in the miniband structure of graphene, which gives rise to new optical interband transitions between VHS which are ultimately reflected in the experimental optical conductivity and interband plasmons. In particular, particle-hole asymmetric features in optical conductivity and plasmons emerged due to moiré potential breaking the symmetry of electronic wavefunction in graphene-hBN structure. The moiré-induced interband plasmons and intrinsic intraband plasmon can coexist in graphene-based non-twisted moiré heterostructures. In twisted moiré structures, changing the twist angle results in varying moiré lengths, leading to a reshaping of the band structure and alterations in both bandwidth and band velocity. In most studies on TBG, the optical absorption peaks and plasmon wavelengths exhibit a red shift as the twist angle decreases. Additionally, interband plasmons, low-damped, and slow plasmon modes have been theoretically explored in flat-band TBG and confirmed by experiments. These findings have spurred further investigations into plasmonics in flat-band twisted trilayer graphene, double bilayer graphene, and twisted TMD systems. Twisting is also recognized as a means to modulate the optical response in other twisted 2D moiré systems that also exhibit intriguing optical phenomena. In flat-band moiré structures, electron-electron interactions can also have an impact on the optical response. Some studies have focused on understanding the effects of these interactions through optical dynamics and plasmonics. Additionally, the formation of superconducting electron pairs through plasmon and electron-electron interactions under the random phase approximation provides insights into the mechanisms underlying superconductivity in moiré structures.

Prosperous and tremendous theoretical and experimental studies on moiré structures are still ongoing to open new avenues for physics and potential applications. Twist-angle induced moiré potentials are appearing in other structures, such as moiré of moiré graphene layers [268–270], TBG-hBN heterostrucuture [271–274], TBG-TMDC heterostructure [27], twisted three-dimensional systems [275–277], and so on. Beyond aforementioned non-twisted moiré heterostructures, studies of MoS_2-metal moiré systems [278], and non-twisted TMDC bilayer moiré heterostructures such as $MoTe_2/WSe_2$ are also arising [279, 280]. These moiré structures could also be ideal platforms for exploring interesting linear and non-linear optical properties as well as plasmonics. For example, spin-orbit coupling accompanying with the moiré potentials could cause more optical transitions in TBG-TMDC systems; the hBN induced band gap could change the plasmon energy in TBG-hBN moiré structures. In addition, the

twist-angle and electron-electron interaction effect can also be important in aligned graphene-based heterostructures in prospective studies. Disorder effects, such as twist-angle and strain effects, have shown an impact on electronic and transport properties in moiré structures [281–285]. More studies of disorder effects on optical properties of moiré structures are also needed in future. Last but not least, although the optical and plasmonic applications of moiré structures are not the primary focus of this topic review they deserve further investigation and attention.

Finally, by creating moiré patterns and further tuning them as needed (e.g., by adjusting the twist angle, combining different materials, and applying artificial structure potentials [286]), we can obtain control over the manipulation of light in future state-of-the-art technologies. This control may find applications in moiré photonics and moiré optoelectronics, including lasers, detectors, modulators, infrared/terahertz photoresponses, and polarizers. Exploring and gaining a fundamental understanding of how the moiré potential influences the optoelectronic properties of these materials is, therefore, crucial for the advancement of the field.

Data availability statement

Any data that support the findings of this study are included within the article.

Acknowledgements

We thank Tommaso Cea, Alejandro Jimeno-Pozo, Héctor Sainz-Cruz, Yunhai Li, Zewen Wu, Yonggang Li for fruitful discussions.IMDEA Nanociencia acknowledges support from the "Severo Ochoa" Programme for Centres of Excellence in R&D (CEX2020-001039-S / AEI / 10.13039/501100011033). P.A.P and F.G. acknowledge funding from the European Commission, within the Graphene Flagship, Core 3, grant number 881603 and from grants NMAT2D (Comunidad de Madrid, Spain), SprQuMat and (MAD2D-CM)-MRR MATERIALES AVANZADOS-IMDEA-NC. S.Y. acknowledges support funding from the National Natural Science Foundation of China (No 12174291) and Natural Science Foundation of Hubei Province, China (Grant No. 2022BAA017). Z.Z. acknowledges support funding from the European Union's Horizon 2020 research and innovation programme under the Marie Skłodowska-Curie grant agreement No 101034431 and from the "Severo Ochoa" Programme for Centres of Excellence in R&D (CEX2020-001039-S / AEI / 10.13039/501100011033).

[1] Novoselov K S, Geim A K, Morozov S V, Jiang D e, Zhang Y, Dubonos S V, Grigorieva I V and Firsov A A 2004 *Science* **306** 666–669 URL https://doi.org/10.1126/science.1102896

[2] Lin Y, Williams T V and Connell J W 2010 *Journal of Physical Chemistry Letters* **1** 277–283 URL https://doi.org/10.1021/jz9002108

[3] Weng Q, Wang X, Wang X, Bando Y and Golberg D 2016 *Chemical Society Reviews* **45** 3989–4012 URL https://doi.org/10.1039/C5CS00869G
[4] Chhowalla M, Shin H S, Eda G, Li L J, Loh K P and Zhang H 2013 *Nature Chemistry* **5** 263–275 URL https://doi.org/10.1038/nchem.1589
[5] Manzeli S, Ovchinnikov D, Pasquier D, Yazyev O V and Kis A 2017 *Nature Reviews Materials* **2** URL https://doi.org/10.1038/natrevmats.2017.33
[6] Li L, Yu Y, Ye G J, Ge Q, Ou X, Wu H, Feng D, Chen X H and Zhang Y 2014 *Nature Nanotechnology* **9** 372–377 URL http://doi.org/10.1038/nnano.2014.35
[7] Ji J, Song X, Liu J, Yan Z, Huo C, Zhang S, Su M, Liao L, Wang W, Ni Z *et al.* 2016 *Nature Communications* **7** 13352 URL https://doi.org/10.1038/ncomms13352
[8] Roldán R, Chirolli L, Prada E, Silva-Guillén J A, San-Jose P and Guinea F 2017 *Chemical Society Reviews* **46** 4387–4399 URL https://doi.org/10.1039/C7CS00210F
[9] Geim A K and Grigorieva I V 2013 *Nature* **499** 419–425 URL http://doi.org/10.1038/nature12385
[10] Dean C, Young A, Wang L, Meric I, Lee G H, Watanabe K, Taniguchi T, Shepard K, Kim P and Hone J 2012 *Solid State Communications* **152** 1275–1282 URL https://doi.org/10.1016/j.ssc.2012.04.021
[11] Andrei E Y and MacDonald A H 2020 *Nature Materials* **19** 1265–1275 URL https://doi.org/10.1038/s41563-020-00840-0
[12] Andrei E Y, Efetov D K, Jarillo-Herrero P, MacDonald A H, Mak K F, Senthil T, Tutuc E, Yazdani A and Young A F 2021 *Nature Reviews Materials* **6** 201–206 URL https://doi.org/10.1038/s41578-021-00284-1
[13] Suárez Morell E, Correa J D, Vargas P, Pacheco M and Barticevic Z 2010 *Physical Review B* **82** 125413 URL https://doi.org/10.1103/PhysRevB.82.121407
[14] Bistritzer R and MacDonald A H 2011 *Proceedings of the National Academy of Sciences* **108** 12233–12237 URL http://doi.org/10.1073/pnas.1108174108
[15] Cao Y, Fatemi V, Fang S, Watanabe K, Taniguchi T, Kaxiras E and Jarillo-Herrero P 2018 *Nature* **556** 43–50 URL https://doi.org/10.1038/nature26160
[16] Yankowitz M, Chen S, Polshyn H, Zhang Y, Watanabe K, Taniguchi T, Graf D, Young A F and Dean C R 2019 *Science* **363** 1059–1064 URL https://doi.org/10.1126/science.aav1910
[17] Oh M, Nuckolls K P, Wong D, Lee R L, Liu X, Watanabe K, Taniguchi T and Yazdani A 2021 *Nature* **600** 240–245 URL http://doi.org/10.1038/s41586-021-04121-x
[18] Cao Y, Fatemi V, Demir A, Fang S, Tomarken S L, Luo J Y, Sanchez-Yamagishi J D, Watanabe K, Taniguchi T, Kaxiras E *et al.* 2018 *Nature* **556** 80–84 URL https://doi.org/10.1038/nature26154
[19] Choi Y, Kemmer J, Peng Y, Thomson A, Arora H, Polski R, Zhang Y, Ren H, Alicea J and Refael G e a 2019 *Nature Physics* **15** 1174–1180 URL https://doi.org/10.1038/s41567-019-0606-5
[20] Xie Y, Lian B, Jäck B, Liu X, Chiu C L, Watanabe K, Taniguchi T, Bernevig B A and Yazdani A 2019 *Nature* **572** 101–105 URL https://doi.org/10.1038/s41586-019-1422-x
[21] Kerelsky A, McGilly L J, Kennes D M, Xian L, Yankowitz M, Chen S, Watanabe K, Taniguchi T, Hone J, Dean C, Rubio A and Pasupathy A N 2019 *Nature* **572** 95–100 URL https://doi.org/10.1038/s41586-019-1431-9
[22] Liu X, Wang Z, Watanabe K, Taniguchi T, Vafek O and Li J I 2021 *Science* **371** 1261–1265 URL https://doi.org/10.1126/science.abb8754
[23] Xie Y, Pierce A T, Park J M, Parker D E, Khalaf E, Ledwith P, Cao Y, Lee S H, Chen S, Forrester P R, Watanabe K, Taniguchi T, Vishwanath A, Jarillo-Herrero P and Yacoby A 2021 *Nature* **600** 439–443 URL https://doi.org/10.1038/s41586-021-04002-3
[24] Choi Y, Kim H, Peng Y, Thomson A, Lewandowski C, Polski R, Zhang Y, Arora H S, Watanabe K, Taniguchi T, Alicea J and Nadj-Perge S 2021 *Nature* **589** 536–541 URL http://doi.org/10.1038/s41586-020-03159-7

[25] Pons R, Mielke A and Stauber T 2020 *Physical Review B* **102** 235101 URL https://doi.org/10.1103/PhysRevB.102.235101
[26] Bhowmik S, Ghawri B, Park Y, Lee D, Datta S, Soni R, Watanabe K, Taniguchi T, Ghosh A, Jung J *et al.* 2023 *Nature Communications* **14** 4055 URL https://doi.org/10.1038/s41467-023-39855-x
[27] Lin J X, Zhang Y H, Morissette E, Wang Z, Liu S, Rhodes D, Watanabe K, Taniguchi T, Hone J and Li J I A 2022 *Science* **375** 437–441 URL http://doi.org/10.1126/science.abh2889
[28] Li Z and Wang Z 2020 *Chinese Physics B* **29** 107101 URL https://doi.org/10.1088/1674-1056/abab77
[29] Tseng C C, Ma X, Liu Z, Watanabe K, Taniguchi T, Chu J H and Yankowitz M 2022 *Nature Physics* **18** 1038–1042 URL https://doi.org/10.1038/s41567-022-01697-7
[30] Duan J, Jian Y, Gao Y, Peng H, Zhong J, Feng Q, Mao J and Yao Y 2022 *Physical Review Letters* **129** 186801 URL https://doi.org/10.1103/PhysRevLett.129.186801
[31] Zhu Z, Carr S, Massatt D, Luskin M and Kaxiras E 2020 *Physical Review Letters* **125** 116404 URL https://doi.org/10.1103/PhysRevLett.125.116404
[32] Park Y, Chittari B L and Jung J 2020 *Physical Review B* **102** 1–14 URL https://doi.org/10.1103/PhysRevB.102.035411
[33] Wu Z, Zhan Z and Yuan S 2021 *Science China Physics, Mechanics & Astronomy* **64** 267811 URL https://doi.org/10.1007/s11433-020-1690-4
[34] Chebrolu N R, Chittari B L and Jung J 2019 *Physical Review B* **99** 235417 URL https://doi.org/10.1103/PhysRevB.99.235417
[35] Rickhaus P, Zheng G, Lado J L, Lee Y, Kurzmann A, Eich M, Pisoni R, Tong C, Garreis R, Gold C, Masseroni M, Taniguchi T, Wantanabe K, Ihn T and Ensslin K 2019 *Nano Letters* **19** 8821–8828 URL https://doi.org/10.1021/acs.nanolett.9b03660
[36] Haddadi F, Wu Q S, Kruchkov A J and Yazyev O V 2020 *Nano Letters* **20** 2410–2415 URL https://doi.org/10.1021/acs.nanolett.9b05117
[37] Rickhaus P, De Vries F K, Zhu J, Portoles E, Zheng G, Masseroni M, Kurzmann A, Taniguchi T, Watanabe K, MacDonald A H, Ihn T and Ensslin K 2021 *Science* **373** 1257–1260 URL https://doi.org/10.1126/science.abc3534
[38] Naik M H and Jain M 2018 *Physical Review Letters* **121** 266401 URL https://doi.org/10.1103/PhysRevLett.121.266401
[39] Venkateswarlu S, Honecker A and Trambly De Laissardière G 2020 *Physical Review B* **102** 81103 URL https://doi.org/10.1103/PhysRevB.102.081103
[40] Zhan Z, Zhang Y, Lv P, Zhong H, Yu G, Guinea F, Silva-Guillén J Á and Yuan S 2020 *Physical Review B* **102** 241106 URL https://doi.org/10.1103/PhysRevB.102.241106
[41] Vitale V, Atalar K, Mostofi A A and Lischner J 2021 *2D Materials* **8** 045010 URL https://doi.org/10.1088/2053-1583/ac15d9
[42] Shabani S, Halbertal D, Wu W, Chen M, Liu S, Hone J, Yao W, Basov D N, Zhu X and Pasupathy A N 2021 *Nature Physics* URL http://dx.doi.org/10.1038/s41567-021-01174-7
[43] Devakul T, Crépel V, Zhang Y and Fu L 2021 *Nature Communications* **12** 6730 URL https://doi.org/10.1038/s41467-021-27042-9
[44] Zhang Y, Liu T and Fu L 2021 *Physical Review B* **103** 155142 URL https://doi.org/10.1103/PhysRevB.103.155142
[45] Xian L, Kennes D M, Tancogne-Dejean N, Altarelli M and Rubio A 2019 *Nano Letters* **19** 4934–4940 URL https://doi.org/10.1021/acs.nanolett.9b00986
[46] Zhao X J, Yang Y, Zhang D B and Wei S H 2020 *Physical Review Letters* **124** 086401 URL https://link.aps.org/doi/10.1103/PhysRevLett.124.086401
[47] Walet N R and Guinea F 2021 *Physical Review B* **103** 125427 URL https://link.aps.org/doi/10.1103/PhysRevB.103.125427
[48] Woods C R, Ares P, Nevison-Andrews H, Holwill M J, Fabregas R, Guinea F, Geim A K, Novoselov K S, Walet N R and Fumagalli L 2021 *Nature Communications* **12** 347 URL

http://doi.org/10.1038/s41467-020-20667-2
[49] Cao Y, Rodan-Legrain D, Rubies-Bigorda O, Park J M, Watanabe K, Taniguchi T and Jarillo-Herrero P 2020 *Nature* **583** 215–220 URL http://dx.doi.org/10.1038/s41586-020-2260-6
[50] Shen C, Chu Y, Wu Q, Li N, Wang S, Zhao Y, Tang J, Liu J, Tian J, Watanabe K *et al.* 2020 *Nature Physics* **16** 520–525 URL https://doi.org/10.1038/s41567-020-0825-9
[51] Park J M, Cao Y, Watanabe K, Taniguchi T and Jarillo-Herrero P 2021 *Nature* **590** 249–255 URL https://doi.org/10.1038/s41586-021-03192-0
[52] He M, Li Y, Cai J, Liu Y, Watanabe K, Taniguchi T, Xu X and Yankowitz M 2021 *Nature Physics* **17** 26–30 URL https://doi.org/10.1038/s41567-020-1030-6
[53] Kim H, Choi Y, Lewandowski C, Thomson A, Zhang Y, Polski R, Watanabe K, Taniguchi T, Alicea J and Nadj-Perge S 2022 *Nature* **606** 494–500 URL https://doi.org/10.1038/s41586-022-04715-z
[54] Hao Z, Zimmerman A, Ledwith P, Khalaf E, Najafabadi D H, Watanabe K, Taniguchi T, Vishwanath A and Kim P 2021 *Science* **371** 1133–1138 URL https://doi.org/10.1126/science.abg0399
[55] Chen S, He M, Zhang Y H, Hsieh V, Fei Z, Watanabe K, Taniguchi T, Cobden D H, Xu X, Dean C R *et al.* 2021 *Nature Physics* **17** 374–380 URL https://doi.org/10.1038/s41567-020-01062-6
[56] Park J M, Cao Y, Xia L Q, Sun S, Watanabe K, Taniguchi T and Jarillo-Herrero P 2022 *Nature Materials* **21** 877–883 URL https://doi.org/10.1038/s41563-022-01287-1
[57] Zhang Y, Polski R, Lewandowski C, Thomson A, Peng Y, Choi Y, Kim H, Watanabe K, Taniguchi T, Alicea J, von Oppen F, Refael G and Nadj-Perge S 2022 *Science* **377** 1538–1543 URL https://doi.org/10.1126/science.abn8585
[58] Burg G W, Khalaf E, Wang Y, Watanabe K, Taniguchi T and Tutuc E 2022 *Nature Materials* **21** 884–889 URL https://doi.org/10.1038/s41563-022-01286-2
[59] Zhu G Y, Xiang T and Zhang G M 2018 *Science Bulletin* **63** 1087–1091 URL https://doi.org/10.1016/j.scib.2018.06.022
[60] Chen G, Jiang L, Wu S, Lyu B, Li H, Chittari B L, Watanabe K, Taniguchi T, Shi Z, Jung J, Zhang Y and Wang F 2019 *Nature Physics* **15** 237–241 URL http://dx.doi.org/10.1038/s41567-018-0387-2
[61] Chittari B L, Chen G, Zhang Y, Wang F and Jung J 2019 *Physical Review Letters* **122** 16401 URL https://doi.org/10.1103/PhysRevLett.122.016401
[62] Chen G, Sharpe A L, Fox E J, Zhang Y H, Wang S, Jiang L, Lyu B, Li H, Watanabe K, Taniguchi T *et al.* 2020 *Nature* **579** 56–61 URL https://doi.org/10.1038/s41586-020-2049-7
[63] Sun X, Zhang S, Liu Z, Zhu H, Huang J, Yuan K, Wang Z, Watanabe K, Taniguchi T, Li X *et al.* 2021 *Nature Communications* **12** 7196 URL https://doi.org/10.1038/s41467-021-27514-y
[64] Wang L, Shih E M, Ghiotto A, Xian L, Rhodes D A, Tan C, Claassen M, Kennes D M, Bai Y, Kim B, Watanabe K, Taniguchi T, Zhu X, Hone J, Rubio A, Pasupathy A N and Dean C R 2020 *Nature Materials* **19** 861–866 URL http://doi.org/10.1038/s41563-020-0708-6
[65] Zhang Z, Wang Y, Watanabe K, Taniguchi T, Ueno K, Tutuc E and LeRoy B J 2020 *Nature Physics* **16** 1093–1096 URL http://doi.org/10.1038/s41567-020-0958-x
[66] Zang J, Wang J, Cano J and Millis A J 2021 *Physical Review B* **104** 075150 URL https://doi.org/10.1103/PhysRevB.104.075150
[67] Xu Y, Kang K, Watanabe K, Taniguchi T and Mak K F 2022 *Nature Nanotechnology* **17** 934–939 URL https://doi.org/10.1038/s41565-022-01180-7
[68] Cai J, Anderson E, Wang C, Zhang X, Liu X, Holtzmann W, Zhang Y, Fan F, Taniguchi T, Watanabe K *et al.* 2023 *Nature* 1–3 URL https://doi.org/10.1038/s41586-023-06289-w
[69] Zeng Y, Xia Z, Kang K, Zhu J, Knüppel P, Vaswani C, Watanabe K, Taniguchi T, Mak K F and Shan J 2023 *Nature* **622** 69–73 URL https://doi.org/10.1038/s41586-023-06452-3
[70] Park H, Cai J, Anderson E, Zhang Y, Zhu J, Liu X, Wang C, Holtzmann W, Hu C, Liu Z *et al.*

2023 *Nature* 1–3 URL https://doi.org/10.1038/s41586-023-06536-0

[71] Xu F, Sun Z, Jia T, Liu C, Xu C, Li C, Gu Y, Watanabe K, Taniguchi T, Tong B *et al.* 2023 *Physical Review X* **13** 031037 URL https://doi.org/10.1103/PhysRevX.13.031037

[72] Andersen T I, Scuri G, Sushko A, De Greve K, Sung J, Zhou Y, Wild D S, Gelly R J, Heo H, Bérubé D, Joe A Y, Jauregui L A, Watanabe K, Taniguchi T, Kim P, Park H and Lukin M D 2021 *Nature Materials* **20** 480–487 URL https://doi.org/10.1038/s41563-020-00873-5

[73] Du L, Molas M R, Huang Z, Zhang G, Wang F and Sun Z 2023 *Science* **379** eadg0014 URL https://doi.org/10.1126/science.adg0014

[74] Mak K F, Sfeir M Y, Wu Y, Lui C H, Misewich J A and Heinz T F 2008 *Physical Review Letters* **101** 196405 URL https://doi.org/10.1103/PhysRevLett.101.196405

[75] Mak K F, Ju L, Wang F and Heinz T F 2012 *Solid State Communications* **152** 1341–1349 URL https://doi.org/10.1016/j.ssc.2012.04.064

[76] Rukelj Z, Štrkalj A and Despoja V 2016 *Physical Review B* **94** 1–11 URL https://link.aps.org/doi/10.1103/PhysRevB.94.115428

[77] Johari P and Shenoy V B 2011 *ACS Nano* **5** 5903–5908 URL https://doi.org/10.1021/nn201698t

[78] Li Y, Chernikov A, Zhang X, Rigosi A, Hill H M, Van Der Zande A M, Chenet D A, Shih E M, Hone J and Heinz T F 2014 *Physical Review B* **90** 205422 URL https://doi.org/10.1103/PhysRevB.90.205422

[79] Laturia A, Van de Put M L and Vandenberghe W G 2018 *npj 2D Materials and Applications* **2** 6 URL https://doi.org/10.1038/s41699-018-0050-x

[80] Scholz A, Stauber T and Schliemann J 2013 *Physical Review B* **88** 035135 URL https://doi.org/10.1103/PhysRevB.88.035135

[81] Cox J D, Silveiro I and García de Abajo F J 2016 *ACS nano* **10** 1995–2003 URL https://doi.org/10.1021/acsnano.5b06110

[82] Koppens F H, Chang D E and García de Abajo F J 2011 *Nano letters* **11** 3370–3377 URL https://doi.org/10.1021/nl201771h

[83] Xiao S, Zhu X, Li B H and Mortensen N A 2016 *Frontiers of Physics* **11** 1–13 URL https://link.springer.com/article/10.1007/s11467-016-0551-z

[84] Gonçalves P A D and Peres N M 2016 *An introduction to graphene plasmonics* (World Scientific) URL https://doi.org/10.1142/9948

[85] Reserbat-Plantey A, Epstein I, Torre I, Costa A T, Gonçalves P, Mortensen N A, Polini M, Song J C, Peres N M and Koppens F H 2021 *Acs Photonics* **8** 85–101 URL https://pubs.acs.org/doi/10.1021/acsphotonics.0c01224

[86] Low T and Avouris P 2014 *ACS Nano* **8** 1086–1101 URL https://doi.org/10.1021/nn406627u

[87] Vakil A and Engheta N 2011 *Science* **332** 1291–1294 URL https://doi.org/10.1126/science.1202691

[88] Stauber T 2014 *Journal of Physics: Condensed Matter* **26** 123201 URL https://doi.org/10.1088/0953-8984/26/12/123201

[89] Wang Y, Ou J Z, Chrimes A F, Carey B J, Daeneke T, Alsaif M M, Mortazavi M, Zhuiykov S, Medhekar N, Bhaskaran M, Friend J R, Strano M S and Kalantar-Zadeh K 2015 *Nano Letters* **15** 883–890 URL https://doi.org/10.1021/nl503563g

[90] Groenewald R, Rösner M, Schönhoff G, Haas S and Wehling T 2016 *Physical Review B* **93** 205145 URL https://doi.org/10.1103/PhysRevB.93.205145

[91] Li Y, Li Z, Chi C, Shan H, Zheng L and Fang Z 2017 *Advanced Science* **4** 1600430 URL https://doi.org/10.1002/advs.201600430

[92] Torbatian Z and Asgari R 2017 *Journal of Physics: Condensed Matter* **29** 465701 URL https://doi.org/10.1088/1361-648X/aa86b9

[93] Sunku S S, McLeod A S, Stauber T, Yoo H, Halbertal D, Ni G, Sternbach A, Jiang B Y, Taniguchi T, Watanabe K *et al.* 2020 *Nano Letters* **20** 2958–2964 URL https://doi.org/10.1021/acs.nanolett.9b04637

[94] Catarina G, Amorim B, Castro E V, Lopes J and Peres N 2019 *Handbook of Graphene* **3** 177–232 URL https://api.semanticscholar.org/CorpusID:199441862

[95] Deng B, Ma C, Wang Q, Yuan S, Watanabe K, Taniguchi T, Zhang F and Xia F 2020 *Nature Photonics* **14** 549–553 URL https://doi.org/10.1038/s41566-020-0644-7

[96] Aizpurua J, Taubner T, de Abajo F J G, Brehm M and Hillenbrand R 2008 *Optics Express* **16** 1529–1545 URL https://doi.org/10.1364/OE.16.001529

[97] Ni G X, Wang H, Wu J S, Fei Z, Goldflam M D, Keilmann F, Özyilmaz B, Castro Neto A H, Xie X M, Fogler M M and Basov D N 2015 *Nature Materials* **14** 1217–1222 URL https://doi.org/10.1038/nmat4425

[98] Hesp N C, Torre I, Rodan-Legrain D, Novelli P, Cao Y, Carr S, Fang S, Stepanov P, Barcons-Ruiz D, Herzig Sheinfux H, Watanabe K, Taniguchi T, Efetov D K, Kaxiras E, Jarillo-Herrero P, Polini M and Koppens F H 2021 *Nature Physics* **17** 1162–1168 URL http://doi.org/10.1038/s41567-021-01327-8

[99] Polman A, Kociak M and García de Abajo F J 2019 *Nature Materials* **18** 1158–1171 URL https://doi.org/10.1038/s41563-019-0409-1

[100] Yan X, Liu C, Gadre C A, Gu L, Aoki T, Lovejoy T C, Dellby N, Krivanek O L, Schlom D G, Wu R *et al.* 2021 *Nature* **589** 65–69 URL https://doi.org/10.1038/s41586-020-03049-y

[101] Sunku S S, Ni G X, Jiang B Y, Yoo H, Sternbach A, Mcleod A S, Stauber T, Xiong L, Taniguchi T, Watanabe K, Kim P, Fogler M M and Basov D N 2018 *Science* **1156** 1153–1156 URL http://dx.doi.org/10.1126/science.aau5144

[102] Kubo R 1957 *Journal of the Physical Society of Japan* **12** 570–586 URL https://doi.org/10.1143/JPSJ.12.570

[103] Calderín L, Karasiev V V and Trickey S B 2017 *Computer Physics Communications* **221** 118–142 URL https://doi.org/10.1016/j.cpc.2017.08.008

[104] Yuan S, De Raedt H and Katsnelson M I 2010 *Physical Review B* **82** 115448 URL https://doi.org/10.1103/PhysRevB.82.115448

[105] Li Y, Zhan Z, Kuang X, Li Y and Yuan S 2023 *Computer Physics Communications* **285** 108632 URL https://doi.org/10.1016/j.cpc.2022.108632

[106] Yu G, Wu Z, Zhan Z, Katsnelson M I and Yuan S 2019 *npj Computational Materials* **5** 122 URL https://doi.org/10.1038/s41524-019-0258-0

[107] Ahn S J, Moon P, Kim T H, Kim H W, Shin H C, Kim E H, Cha H W, Kahng S J, Kim P, Koshino M *et al.* 2018 *Science* **361** 782–786 URL https://doi.org/10.1126/science.aar8412

[108] Yao W, Wang E, Bao C, Zhang Y, Zhang K, Bao K, Chan C K, Chen C, Avila J, Asensio M C *et al.* 2018 *Proceedings of the National Academy of Sciences* **115** 6928–6933 URL http://www.pnas.org/cgi/doi/10.1073/pnas.1720865115

[109] Pezzini S, Miseikis V, Piccinini G, Forti S, Pace S, Engelke R, Rossella F, Watanabe K, Taniguchi T, Kim P *et al.* 2020 *Nano letters* **20** 3313–3319 URL https://doi.org/10.1021/acs.nanolett.0c00172

[110] Moon P, Koshino M and Son Y W 2019 *Physical Review B* **99** 165430 URL https://doi.org/10.1103/PhysRevB.99.165430

[111] Yuan S, Roldán R, De Raedt H and Katsnelson M I 2011 *Physical Review B* **84** 195418 URL https://doi.org/10.1103/PhysRevB.84.195418

[112] Roche S 1999 *Physical Review B* **59** 2284 URL https://link.aps.org/doi/10.1103/PhysRevB.59.2284

[113] Fan Z, Garcia J H, Cummings A W, Barrios-Vargas J E, Panhans M, Harju A, Ortmann F and Roche S 2021 *Physics Reports* **903** 1–69 URL https://doi.org/10.1016/j.physrep.2020.12.001

[114] Kuzmenko A 2005 *Review of scientific instruments* **76** URL https://doi.org/10.1063/1.1979470

[115] Moon P and Koshino M 2013 *Physical Review B* **87** 205404 URL https://doi.org/10.1103/PhysRevB.87.205404

[116] Mahan G D 2000 *Many-particle physics* (Springer Science & Business Media) URL https://doi.org/10.1007/978-1-4757-5714-9
[117] Giuliani G and Vignale G 2008 *Quantum theory of the electron liquid* (Cambridge university press) URL https://doi.org/10.1017/CBO9780511619915
[118] Coleman P 2015 *Introduction to many-body physics* (Cambridge University Press) URL https://doi.org/10.1017/CBO9781139020916
[119] Yuan S, Roldán R and Katsnelson M I 2011 *Physical Review B* **84** 35439 URL https://doi.org/10.1103/PhysRevB.84.035439
[120] Kuang X, Zhan Z and Yuan S 2021 *Physical Review B* **103** 115431 URL https://doi.org/10.1103/PhysRevB.103.115431
[121] Stauber T, San-Jose P and Brey L 2013 *New Journal of Physics* **15** 113050 URL http://doi.org/10.1088/1367-2630/15/11/113050
[122] Maier S A *et al.* 2007 *Plasmonics: fundamentals and applications* vol 1 (Springer) URL https://link.springer.com/book/10.1007/0-387-37825-1
[123] Morawetz K, Ashokan V, Bala R and Pathak K N 2018 *Physical Review B* **97** 155147 URL https://doi.org/10.1103/PhysRevB.97.155147
[124] Kotov V N, Uchoa B and Neto A C 2008 *Physical Review B* **78** 035119 URL https://link.aps.org/doi/10.1103/PhysRevB.78.035119
[125] Sabio J, Nilsson J and Neto A C 2008 *Physical Review B* **78** 075410 URL https://link.aps.org/doi/10.1103/PhysRevB.78.075410
[126] Abedinpour S H, Vignale G, Principi A, Polini M, Tse W K and MacDonald A 2011 *Physical Review B* **84** 045429 URL https://link.aps.org/doi/10.1103/PhysRevB.84.045429
[127] Gangadharaiah S, Farid A and Mishchenko E 2008 *Physical review letters* **100** 166802 URL https://link.aps.org/doi/10.1103/PhysRevLett.100.166802
[128] Inaoka T, Nagao T, Hasegawa S, Hildebrandt T and Henzler M 2002 *Physical Review B* **66** 245320 URL https://doi.org/10.1103/PhysRevB.66.245320
[129] Singwi K, Tosi M, Land R and Sjölander A 1968 *Physical Review* **176** 589 URL https://link.aps.org/doi/10.1103/PhysRev.176.589
[130] Jonson M 1976 *Journal of Physics C: Solid State Physics* **9** 3055 URL https://iopscience.iop.org/article/10.1088/0022-3719/9/16/012
[131] Neilson D, Świerkowski L, Sjölander A and Szymański J 1991 *Physical Review B* **44** 6291 URL https://link.aps.org/doi/10.1103/PhysRevB.44.6291
[132] March N and Tosi M 1995 *Advances in Physics* **44** 299–386 URL https://doi.org/10.1080/00018739500101546
[133] Adler S L 1962 *Physical Review* **126** 413 URL https://doi.org/10.1103/PhysRev.126.413
[134] Wiser N 1963 *Physical Review* **129** 62 URL https://doi.org/10.1103/PhysRev.129.62
[135] Louie S G, Chelikowsky J R and Cohen M L 1975 *Physical Review Letters* **34** 155 URL https://doi.org/10.1103/PhysRevLett.34.155
[136] Van Vechten J and Martin R M 1972 *Physical Review Letters* **28** 446 URL https://doi.org/10.1103/PhysRevLett.28.446
[137] Sturm K 1978 *Physical Review Letters* **40** 1599 URL https://doi.org/10.1103/PhysRevLett.40.1599
[138] Yang L, Deslippe J, Park C H, Cohen M L and Louie S G 2009 *Physical Review Letters* **103** 186802 URL https://link.aps.org/doi/10.1103/PhysRevLett.103.186802
[139] Xue J, Sanchez-Yamagishi J, Bulmash D, Jacquod P, Deshpande A, Watanabe K, Taniguchi T, Jarillo-Herrero P and LeRoy B J 2011 *Nature Materials* **10** 282–285 URL https://doi.org/10.1038/nmat2968
[140] Wang L, Zihlmann S, Liu M H, Makk P, Watanabe K, Taniguchi T, Baumgartner A and Schonenberger C 2019 *Nano Letters* **19** 2371–2376 URL https://doi.org/10.1021/acs.nanolett.8b05061
[141] Wang E, Lu X, Ding S, Yao W, Yan M, Wan G, Deng K, Wang S, Chen G, Ma L *et al.* 2016

Nature Physics **12** 1111–1115 URL https://doi.org/10.1038/nphys3856
[142] Shi Z, Jin C, Yang W, Ju L, Horng J, Lu X, Bechtel H A, Martin M C, Fu D, Wu J *et al.* 2014 *Nature Physics* **10** 743–747 URL https://doi.org/10.1038/nphys3075
[143] Wallbank J R, Patel A A, Mucha-Kruczyński M, Geim A K and Fal'ko V I 2013 *Phys. Rev. B* **87**(24) 245408 URL https://link.aps.org/doi/10.1103/PhysRevB.87.245408
[144] Nakagahara K and Wakabayashi K 2022 *Physical Review B* **106** 075403 URL https://doi.org/10.1103/PhysRevB.106.075403
[145] DaSilva A M, Jung J, Adam S and MacDonald A H 2015 *Physical Review B* **92** 155406 URL https://link.aps.org/doi/10.1103/PhysRevB.92.155406
[146] Abergel D S and Mucha-Kruczyński M 2015 *Physical Review B* **92** 115430 URL https://link.aps.org/doi/10.1103/PhysRevB.92.115430
[147] Liu B, Zhang Y T, Qiao R, Shi R, Li Y, Guo Q, Li J, Li X, Wang L, Qi J *et al.* 2023 *Physical Review Letters* **131** 016201 URL https://doi.org/10.1103/PhysRevLett.131.016201
[148] Hwang E and Sarma S D 2007 *Physical Review B* **75** 205418 URL https://link.aps.org/doi/10.1103/PhysRevB.75.205418
[149] Eberlein T, Bangert U, Nair R R, Jones R, Gass M, Bleloch A L, Novoselov K S, Geim A and Briddon P R 2008 *Physical Review B* **77** 233406 URL https://link.aps.org/doi/10.1103/PhysRevB.77.233406
[150] Tomadin A, Guinea F and Polini M 2014 *Physical Review B* **90** 161406 URL https://link.aps.org/doi/10.1103/PhysRevB.90.161406
[151] Tomadin A, Polini M and Jung J 2019 *Physical Review B* **99** 035432 URL https://doi.org/10.1103/PhysRevB.99.035432
[152] Bandurin D A, Svintsov D, Gayduchenko I, Xu S G, Principi A, Moskotin M, Tretyakov I, Yagodkin D, Zhukov S, Taniguchi T *et al.* 2018 *Nature Communications* **9** 5392 URL http://dx.doi.org/10.1038/s41467-018-07848-w
[153] Yankowitz M, Xue J, Cormode D, Sanchez-Yamagishi J D, Watanabe K, Taniguchi T, Jarillo-Herrero P, Jacquod P and LeRoy B J 2012 *Nature Physics* **8** 382–386 URL https://doi.org/10.1038/nphys2272
[154] Politano A, Slotman G J, Roldán R, Chiarello G, Campi D, Katsnelson M I and Yuan S 2017 *2D Materials* **4** 021001 URL https://doi.org/10.1088/2053-1583/aa53ba
[155] Despoja V, Novko D, Lončarić I, Golenić N, Marušić L and Silkin V M 2019 *Physical Review B* **100** 195401 URL https://doi.org/10.1103/PhysRevB.100.195401
[156] Politano A, Marino A, Formoso V, Farías D, Miranda R and Chiarello G 2011 *Physical Review B* **84** 033401 URL https://doi.org/10.1103/PhysRevB.84.033401
[157] Politano A, Marino A and Chiarello G 2012 *Physical Review B* **86** 085420 URL https://link.aps.org/doi/10.1103/PhysRevB.86.085420
[158] Langer T, Förster D, Busse C, Michely T, Pfnür H and Tegenkamp C 2011 *New Journal of Physics* **13** 053006 URL http://doi.org/10.1088/1367-2630/13/5/053006
[159] Dos Santos J L, Peres N and Neto A C 2007 *Physical Review Letters* **99** 256802 URL https://doi.org/10.1103/PhysRevLett.99.256802
[160] Shallcross S, Sharma S and Pankratov O A 2008 *Physical Review Letters* **101** 056803 URL https://doi.org/10.1103/PhysRevLett.101.056803
[161] Shallcross S, Sharma S, Kandelaki E and Pankratov O 2010 *Physical Review B* **81** 165105 URL https://doi.org/10.1103/PhysRevB.81.165105
[162] Trambly de Laissardière G, Mayou D and Magaud L 2010 *Nano Letters* **10** 804–808 URL https://doi.org/10.1021/nl902948m
[163] Mele E J 2010 *Physical Review B* **81** 161405 URL https://doi.org/10.1103/PhysRevB.81.161405
[164] Dos Santos J L, Peres N and Neto A C 2012 *Physical Review B* **86** 155449 URL https://doi.org/10.1103/PhysRevB.86.155449
[165] Trambly De Laissardière G, Mayou D and Magaud L 2012 *Physical Review B* **86** 125413 ISSN

10980121 URL https://doi.org/10.1103/PhysRevB.86.125413
[166] Lu X, Stepanov P, Yang W, Xie M, Aamir M A, Das I, Urgell C, Watanabe K, Taniguchi T, Zhang G *et al.* 2019 *Nature* **574** 653–657 URL https://doi.org/10.1038/s41586-019-1695-0
[167] Polshyn H, Yankowitz M, Chen S, Zhang Y, Watanabe K, Taniguchi T, Dean C R and Young A F 2019 *Nature Physics* **15** 1011–1016 URL https://doi.org/10.1038/s41567-019-0596-3
[168] Sharpe A L, Fox E J, Barnard A W, Finney J, Watanabe K, Taniguchi T, Kastner M and Goldhaber-Gordon D 2019 *Science* **365** 605–608 URL https://doi.org/10.1126/science.aaw3780
[169] Serlin M, Tschirhart C, Polshyn H, Zhang Y, Zhu J, Watanabe K, Taniguchi T, Balents L and Young A 2020 *Science* **367** 900–903 URL https://doi.org/10.1126/science.aay5533
[170] Saito Y, Ge J, Watanabe K, Taniguchi T and Young A F 2020 *Nature Physics* **16** 926–930 URL https://doi.org/10.1038/s41567-020-0928-3
[171] Zondiner U, Rozen A, Rodan-Legrain D, Cao Y, Queiroz R, Taniguchi T, Watanabe K, Oreg Y, von Oppen F, Stern A *et al.* 2020 *Nature* **582** 203–208 URL https://doi.org/10.1038/s41586-020-2373-y
[172] Wong D, Nuckolls K P, Oh M, Lian B, Xie Y, Jeon S, Watanabe K, Taniguchi T, Bernevig B A and Yazdani A 2020 *Nature* **582** 198–202 URL https://doi.org/10.1038/s41586-020-2339-0
[173] Stepanov P, Das I, Lu X, Fahimniya A, Watanabe K, Taniguchi T, Koppens F H, Lischner J, Levitov L and Efetov D K 2020 *Nature* **583** 375–378 URL https://doi.org/10.1038/s41586-020-2459-6
[174] Xu Y, Liu S, Rhodes D A, Watanabe K, Taniguchi T, Hone J, Elser V, Mak K F and Shan J 2020 *Nature* **587** 214–218 URL https://doi.org/10.1038/s41586-020-2868-6
[175] Rozen A, Park J M, Zondiner U, Cao Y, Rodan-Legrain D, Taniguchi T, Watanabe K, Oreg Y, Stern A, Berg E *et al.* 2021 *Nature* **592** 214–219 URL https://doi.org/10.1038/s41586-021-03319-3
[176] Cao Y, Rodan-Legrain D, Park J M, Yuan N F, Watanabe K, Taniguchi T, Fernandes R M, Fu L and Jarillo-Herrero P 2021 *Science* **372** 264–271 URL https://doi.org/10.1126/science.abc2836
[177] Stepanov P, Xie M, Taniguchi T, Watanabe K, Lu X, MacDonald A H, Bernevig B A and Efetov D K 2021 *Physical Review Letters* **127** 197701 URL https://doi.org/10.1103/PhysRevLett.127.197701
[178] Berdyugin A I, Xin N, Gao H, Slizovskiy S, Dong Z, Bhattacharjee S, Kumaravadivel P, Xu S, Ponomarenko L, Holwill M *et al.* 2022 *Science* **375** 430–433 URL https://doi.org/10.1126/science.abi8627
[179] Turkel S, Swann J, Zhu Z, Christos M, Watanabe K, Taniguchi T, Sachdev S, Scheurer M S, Kaxiras E, Dean C R *et al.* 2022 *Science* **376** 193–199 URL https://doi.org/10.1126/science.abk1895
[180] Yu K, Van Luan N, Kim T, Jeon J, Kim J, Moon P, Lee Y H and Choi E 2019 *Physical Review B* **99** 241405 URL https://doi.org/10.1103/PhysRevB.99.241405
[181] San-Jose P and Prada E 2013 *Physical Review B* **88** 121408 URL https://doi.org/10.1103/PhysRevB.88.121408
[182] Tsim B, Nam N N and Koshino M 2020 *Physical Review B* **101** 125409 URL https://doi.org/10.1103/PhysRevB.101.125409
[183] Moon P, Son Y W and Koshino M 2014 *Physical Review B* **90** 155427 URL https://link.aps.org/doi/10.1103/PhysRevB.90.155427
[184] Zou X, Shang J, Leaw J, Luo Z, Luo L, Cheng L, Cheong S, Su H, Zhu J X, Liu Y *et al.* 2013 *Physical Review Letters* **110** 067401 URL https://doi.org/10.1103/PhysRevLett.110.067401
[185] Calderón M J and Bascones E 2020 *npj Quantum Materials* **5** 57 URL http://dx.doi.org/10.1038/s41535-020-00258-6
[186] Tabert C J and Nicol E J 2013 *Physical Review B* **87** 121402 URL https://doi.org/10.1103/

PhysRevB.87.121402
[187] Havener R W, Liang Y, Brown L, Yang L and Park J 2014 *Nano Letters* **14** 3353–3357 URL https://doi.org/10.1021/nl500823k
[188] Novelli P, Torre I, Koppens F H, Taddei F and Polini M 2020 *Physical Review B* **102** 125403 URL http://dx.doi.org/10.1103/PhysRevB.102.125403
[189] Dai Z B, He Y and Li Z 2021 *Physical Review B* **104** 045403 URL https://doi.org/10.1103/PhysRevB.104.045403
[190] Moon P and Koshino M 2013 *Physical Review B* **88** 241412 URL https://doi.org/10.1103/PhysRevB.88.241412
[191] Natalin N, Kundelev E, Rukhlenko I D and Tepliakov N 2023 *Electronic Structure* URL https://doi.org/10.1088/2516-1075/acdbf5
[192] Chang K, Zheng Z, Sipe J E and Cheng J L 2022 *Physical Review B* **106** 1–11 URL https://doi.org/10.1103/PhysRevB.106.245405
[193] Wang Y, Ni Z, Liu L, Liu Y, Cong C, Yu T, Wang X, Shen D and Shen Z 2010 *ACS Nano* **4** 4074–4080 URL https://doi.org/10.1021/nn1004974
[194] Vela A, Moutinho M, Culchac F, Venezuela P and Capaz R B 2018 *Physical Review B* **98** 155135 URL https://doi.org/10.1103/PhysRevB.98.155135
[195] Wang Y, Yu G, Rösner M, Katsnelson M I, Lin H Q and Yuan S 2021 *Physical Review X* **12** 21055 URL http://doi.org/10.1103/PhysRevX.12.021055
[196] Ochoa H and Asenjo-Garcia A 2020 *Physical Review Letters* **125** 37402 URL https://doi.org/10.1103/PhysRevLett.125.037402
[197] Lee H Y, Al Ezzi M M, Raghuvanshi N, Chung J Y, Watanabe K, Taniguchi T, Garaj S, Adam S and Gradecak S 2021 *Nano Letters* **21** 2832–2839 URL https://pubs.acs.org/doi/10.1021/acs.nanolett.0c04924
[198] Zhao S, Wang E, Üzer E A, Guo S, Qi R, Tan J, Watanabe K, Taniguchi T, Nilges T, Gao P, Zhang Y, Cheng H m, Liu B, Zou X and Wang F 2021 *Nature Communications* 6–12 URL http://dx.doi.org/10.1038/s41467-021-24272-9
[199] Wu X, Fu C and Zhang Z M 2019 *Optics Communications* **452** 124–129 URL https://doi.org/10.1016/j.optcom.2019.07.015
[200] Qiao J, Kong X, Hu Z X, Yang F and Ji W 2014 *Nature communications* **5** 4475 URL https://doi.org/10.1038/ncomms5475
[201] Li L, Kim J, Jin C, Ye G J, Qiu D Y, Da Jornada F H, Shi Z, Chen L, Zhang Z, Yang F *et al.* 2017 *Nature nanotechnology* **12** 21–25 URL https://doi.org/10.1038/nnano.2016.171
[202] Khaliji K, Martín-Moreno L, Avouris P, Oh S H and Low T 2022 *Physical Review Letters* **128** 193902 URL https://doi.org/10.1103/PhysRevLett.128.193902
[203] Lee S, Seo D, Park S H, Izquierdo N, Lee E H, Younas R, Zhou G, Palei M, Hoffman A J, Jang M S *et al.* 2023 *Nature Communications* **14** 3889 URL https://doi.org/10.1038/s41467-023-39450-0
[204] Stauber T and Kohler H 2016 *Nano Letters* **16** 6844–6849 URL https://doi.org/10.1021/acs.nanolett.6b02587
[205] Lewandowski C and Levitov L 2019 *Proceedings of the National Academy of Sciences* **116** 20869–20874 URL https://doi.org/10.1073/pnas.1909069116
[206] Stauber T, Low T and Gómez-Santos G 2018 *Physical Review Letters* **120** 46801 URL https://doi.org/10.1103/PhysRevLett.120.046801
[207] Yin J, Wang H, Peng H, Tan Z, Liao L, Lin L, Sun X, Koh A L, Chen Y, Peng H and Liu Z 2016 *Nature Communications* **7** URL https://doi.org/10.1038/ncomms10699
[208] Patel H, Havener R W, Brown L, Liang Y, Yang L, Park J and Graham M W 2015 *Nano Letters* **15** 5932–5937 URL https://doi.org/10.1021/acs.nanolett.5b02035
[209] Ding C, Gao H, Sun L, Ma X and Zhao M 2021 *Physical Review B* **104** 155427 URL https://doi.org/10.1103/PhysRevB.104.155427
[210] Stern F 1967 *Physical Review Letters* **18** 546 URL https://doi.org/10.1103/PhysRevLett.

18.546
[211] Brey L, Stauber T, Slipchenko T and Martín-Moreno L 2020 *Physical Review Letters* **125** 256804 URL https://doi.org/10.1103/PhysRevLett.125.256804
[212] Zhou M 2021 *Physical Review B* **104** 045419 URL https://doi.org/10.1103/PhysRevB.104.045419
[213] Papaj M and Lewandowski C 2020 *Physical Review Letters* **125** 066801 URL https://doi.org/10.1103/PhysRevLett.125.066801
[214] Song J, Zhang Z, Feng N and Wang J 2021 *Nanomaterials* **11** 2433 URL https://doi.org/10.3390/nano11092433
[215] Lin X, Liu Z, Stauber T, Gómez-Santos G, Gao F, Chen H, Zhang B and Low T 2020 *Physical Review Letters* **125** 077401 URL https://doi.org/10.1103/PhysRevLett.125.077401
[216] Stauber T, Low T and Gómez-Santos G 2020 *Nano Letters* **20** 8711–8718 URL https://doi.org/10.1021/acs.nanolett.0c03519
[217] Margetis D and Stauber T 2021 *Physical Review B* **104** 115422 URL https://doi.org/10.1103/PhysRevB.104.115422
[218] Ding C, Zhang X, Gao H, Ma X, Li Y and Zhao M 2022 *Physical Review B* **106** 155402 ISSN 0031-899X URL https://doi.org/10.1103/PhysRevB.106.155402
[219] Westerhout T, Katsnelson M I and Rösner M 2021 *2D Materials* **9** 014004 URL https://doi.org/10.1088/2053-1583/ac38ca
[220] Do T N, Shih P H and Gumbs G 2023 *Journal of Physics: Condensed Matter* URL https://doi.org/10.1088/1361-648X/acecf1
[221] Hu F, Das S R, Luan Y, Chung T F, Chen Y P and Fei Z 2017 *Physical Review Letters* **119** 247402 URL https://doi.org/10.1103/PhysRevLett.119.247402
[222] Huang T, Tu X, Shen C, Zheng B, Wang J, Wang H, Khaliji K, Park S H, Liu Z, Yang T, Zhang Z, Shao L, Li X, Low T, Shi Y and Wang X 2022 *Nature* **605** 63–68 URL https://doi.org/10.1038/s41586-022-04520-8
[223] Su X, Huang T, Zheng B, Wang J, Wang X, Yan S, Wang X and Shi Y 2022 *Nano Letters* **22** 8975–8982 URL https://doi.org/10.1021/acs.nanolett.2c03220
[224] Wu Z, Kuang X, Zhan Z and Yuan S 2021 *Physical Review B* **104** 205104 URL https://doi.org/10.1103/PhysRevB.104.205104
[225] Chakraborty A, Dutta D and Agarwal A 2022 *Physical Review B* **106** 155422 URL https://doi.org/10.1103/PhysRevB.106.155422
[226] Kuang X, Zhan Z and Yuan S 2022 *Physical Review B* **105** 245415 URL https://doi.org/10.1103/PhysRevB.105.245415
[227] Wang C, Xie Y, Ma J, Hu G, Xing Q, Huang S, Song C, Wang F, Lei Y, Zhang J *et al.* 2023 *Nano Letters* URL https://doi.org/10.1021/acs.nanolett.3c01472
[228] Xiao Y M, Xu W, Peeters F M and Van Duppen B 2017 *Physical Review B* **96** 085405–085420 URL https://doi.org/10.1103/PhysRevB.96.085405
[229] Yang J, Chen G, Han T, Zhang Q, Zhang Y H, Jiang L, Lyu B, Li H, Watanabe K, Taniguchi T, Shi Z, Senthil T, Zhang Y, Wang F and Ju L 2022 *Science* **375** 1295–1299 URL https://doi.org/10.1126/science.abg3036
[230] Papaj M and Lewandowski C 2023 *Science Advances* **9** eadg3262 URL https://doi.org/10.1126/sciadv.adg3262
[231] Otteneder M, Hubmann S, Lu X, Kozlov D A, Golub L E, Watanabe K, Taniguchi T, Efetov D K and Ganichev S D 2020 *Nano Letters* **20** 7152–7158 URL https://doi.org/10.1021/acs.nanolett.0c02474
[232] Ikeda T N 2020 *Physical Review Research* **2** 032015 URL https://link.aps.org/doi/10.1103/PhysRevResearch.2.032015
[233] Herzig Sheinfux H and Koppens F H 2020 *Nano Letters* **20** 6935–6936 URL https://doi.org/10.1021/acs.nanolett.0c03175
[234] Topp G E, Jotzu G, McIver J W, Xian L, Rubio A and Sentef M A 2019 *Physical Review Research*

1 023031 URL https://doi.org/10.1103/physrevresearch.1.023031
[235] Du M, Liu C, Zeng Z and Li R 2021 *Physical Review Research* **104** 033113 URL https://link.aps.org/doi/10.1103/PhysRevA.104.033113
[236] Katz O, Refael G and Lindner N H 2020 *Physical Review B* **102** 155123 URL https://link.aps.org/doi/10.1103/PhysRevB.102.155123
[237] Vogl M, Rodriguez-Vega M and Fiete G A 2020 *Physical Review Research* **101** 241408 URL https://link.aps.org/doi/10.1103/PhysRevB.101.241408
[238] Vogl M, Rodriguez-Vega M and Fiete G A 2020 *Physical Review B* **101** 235411 URL https://link.aps.org/doi/10.1103/PhysRevB.101.235411
[239] Brihuega I, Mallet P, González-Herrero H, De Laissardière G T, Ugeda M, Magaud L, Gómez-Rodríguez J M, Ynduráin F and Veuillen J Y 2012 *Physical Review Letters* **109** 196802 URL https://doi.org/10.1103/PhysRevLett.109.196802
[240] Zuber J W and Zhang C 2021 *Physical Review B* **103** 245417 URL https://link.aps.org/doi/10.1103/PhysRevB.103.245417
[241] Yang F, Song W, Meng F, Luo F, Lou S, Lin S, Gong Z, Cao J, Barnard E S, Chan E, Yang L and Yao J 2020 *Matter* **3** 1361–1376 URL https://doi.org/10.1016/j.matt.2020.08.018
[242] Du L, Dai Y and Sun Z 2020 *Matter* **3** 987–988 URL https://doi.org/10.1016/j.matt.2020.09.013
[243] Di Mauro Villari L and Principi A 2022 *Physical Review B* **106** 035401 URL https://link.aps.org/doi/10.1103/PhysRevB.106.035401
[244] Shimazaki Y, Yamamoto M, Borzenets I V, Watanabe K, Taniguchi T and Tarucha S 2015 *Nature Physics* **11** 1032–1036 URL https://doi.org/10.1038/nphys3551
[245] Gao Y, Zhang Y and Xiao D 2020 *Physical Reveview Letters* **124** 077401 URL https://link.aps.org/doi/10.1103/PhysRevLett.124.077401
[246] Ha S, Park N H, Kim H, Shin J, Choi J, Park S, Moon J Y, Chae K, Jung J, Lee J H, Yoo Y, Park J Y, Ahn K J and Yeom D I 2021 *Light: Science and Applications* **10** URL https://doi.org/10.1038/s41377-020-00459-5
[247] Hu J X, Xie Y M and Law K 2023 *Physical Review B* **107** 075424 URL https://doi.org/10.1103/PhysRevB.107.075424
[248] Molinero E B, Datta A, Calderón M J, Bascones E and Silva R E 2023 *arXiv preprint arXiv:2302.04127* URL http://arxiv.org/abs/2302.04127
[249] Zhang S, Lu X and Liu J 2022 *Physical Review Letters* **128** 1–20 URL https://doi.org/10.1103/PhysRevLett.128.247402
[250] Kim B, Jin J, Wang Z, He L, Christensen T, Mele E J and Zhen B 2023 *Nature Photonics* 1–8 URL https://doi.org/10.1038/s41566-023-01318-6
[251] Stepanov E A, Semin S V, Woods C R, Vandelli M, Kimel A V, Novoselov K S and Katsnelson M I 2020 *ACS Applied Materials and Interfaces* **12** 27758–27764 URL https://doi.org/10.1021/acsami.0c05965
[252] Goodwin Z A, Corsetti F, Mostofi A A and Lischner J 2019 *Physical Review B* **100** 235424 URL https://doi.org/10.1103/PhysRevB.100.235424
[253] Gonzalez J and Stauber T 2019 *Physical Review Letters* **122** 26801 URL https://doi.org/10.1103/PhysRevLett.122.026801
[254] Cea T and Guinea F 2021 *Proceedings of the National Academy of Sciences* **118** e2107874118 URL https://doi.org/10.1073/pnas.2107874118
[255] Sharma G, Trushin M, Sushkov O P, Vignale G and Adam S 2020 *Physical Review Research* **2** 022040 URL https://doi.org/10.1103/PhysRevResearch.2.022040
[256] Lewandowski C, Chowdhury D and Ruhman J 2021 *Physical Review B* **103** 235401 URL https://doi.org/10.1103/PhysRevB.103.235401
[257] Törmä P, Peotta S and Bernevig B A 2022 *Nature Reviews Physics* **4** 528–542 URL https://doi.org/10.1038/s42254-022-00466-y
[258] Wu F, MacDonald A H and Martin I 2018 *Physical Review Letters* **121** 257001 URL https:

//link.aps.org/doi/10.1103/PhysRevLett.121.257001
[259] Lian B, Wang Z and Bernevig B A 2019 *Physical Review Letters* **122** 257002 URL https://doi.org/10.1103/PhysRevLett.122.257002
[260] Peltonen T J, Ojajärvi R and Heikkilä T T 2018 *Physical Review B* **98** 220504 URL https://doi.org/10.1103/PhysRevB.98.220504
[261] Guinea F and Walet N R 2018 *Proceedings of the National Academy of Sciences of the United States of America* **115** 13174–13179 ISSN 10916490 (*Preprint* 1806.05990)
[262] Cea T 2023 *Phys. Rev. B* **107**(4) L041111 URL https://link.aps.org/doi/10.1103/PhysRevB.107.L041111
[263] Cea T, Pantaleón P A, Walet N R and Guinea F 2022 *Nano Materials Science* **4** 27–35 URL https://doi.org/10.1016/j.nanoms.2021.10.001
[264] Peng L, Yudhistira I, Vignale G and Adam S 2023 *arXiv preprint arXiv:2309.14767* URL https://doi.org/10.48550/arXiv.2309.14767
[265] Martin I 2020 *Annals of Physics* **417** 168118 URL https://doi.org/10.1016/j.aop.2020.168118
[266] Migdal A 1958 *Sov. Phys. JETP* **7** 996–1001 URL http://jetp.ras.ru/cgi-bin/dn/e_007_06_0996.pdf
[267] Takada Y 1992 *Journal of the Physical Society of Japan* **61** 3849–3852 URL http://journals.jps.jp/doi/pdf/10.1143/JPSJ.61.3849
[268] Uri A, de la Barrera S C, Randeria M T, Rodan-Legrain D, Devakul T, Crowley P J, Paul N, Watanabe K, Taniguchi T, Lifshitz R *et al.* 2023 *Nature* 1–6 URL https://doi.org/10.1038/s41586-023-06294-z
[269] Devakul T, Ledwith P J, Xia L Q, Uri A, de la Barrera S C, Jarillo-Herrero P and Fu L 2023 *Science Advances* **9** eadi6063 URL https://doi.org/10.1126/sciadv.adi6063
[270] Meng H, Zhan Z and Yuan S 2023 *Physical Review B* **107** 035109
[271] Cea T, Pantaleón P A and Guinea F 2020 *Physical Review B* **102** 155136 URL https://link.aps.org/doi/10.1103/PhysRevB.102.155136
[272] Shi J, Zhu J and MacDonald A 2021 *Physical Review B* **103** 075122 URL https://doi.org/10.1103/PhysRevB.103.075122
[273] Long M, Pantaleón P A, Zhan Z, Guinea F, Silva-Guillén J Á and Yuan S 2022 *npj Computational Materials* **8** 73 URL https://doi.org/10.1038/s41524-022-00763-1
[274] Long M, Zhan Z, Pantaleón P A, Silva-Guillén J A, Guinea F and Yuan S 2023 *Physical Review B* **107** 115140 URL https://link.aps.org/doi/10.1103/PhysRevB.107.115140
[275] Fujimoto M, Kawakami T and Koshino M 2022 *Physical Review Research* **4** 043209 URL https://doi.org/10.1103/PhysRevResearch.4.043209
[276] Song Z, Sun X and Wang L W 2021 *Physical Review B* **103** 245206 URL https://doi.org/10.1103/PhysRevB.103.245206
[277] Mullan C, Slizovskiy S, Yin J, Wang Z, Yang Q, Xu S, Yang Y, Piot B A, Hu S, Taniguchi T *et al.* 2023 *Nature* 1–6 URL https://doi.org/10.1038/s41586-023-06264-5
[278] Reidy K, Varnavides G, Thomsen J D, Kumar A, Pham T, Blackburn A M, Anikeeva P, Narang P, LeBeau J M and Ross F M 2021 *Nature Communications* **12** 1290 URL https://doi.org/10.1038/s41467-021-21363-5
[279] Li T, Jiang S, Shen B, Zhang Y, Li L, Tao Z, Devakul T, Watanabe K, Taniguchi T, Fu L, Shan J and Mak K F 2021 *Nature* **600** 641–646 URL https://doi.org/10.1038/s41586-021-04171-1
[280] Li T, Jiang S, Li L, Zhang Y, Kang K, Zhu J, Watanabe K, Taniguchi T, Chowdhury D, Fu L, Shan J and Mak K F 2021 *Nature* **597** 350–354 URL https://doi.org/10.1038/s41586-021-03853-0
[281] Uri A, Grover S, Cao Y, Crosse J A, Bagani K, Rodan-Legrain D, Myasoedov Y, Watanabe K, Taniguchi T, Moon P *et al.* 2020 *Nature* **581** 47–52 URL https://doi.org/10.1038/s41586-020-2255-3

[282] Kazmierczak N P, Van Winkle M, Ophus C, Bustillo K C, Carr S, Brown H G, Ciston J, Taniguchi T, Watanabe K and Bediako D K 2021 *Nature materials* **20** 956–963 URL https://doi.org/10.1038/s41563-021-00973-w

[283] Wilson J H, Fu Y, Sarma S D and Pixley J 2020 *Physical Review Research* **2** 023325 URL https://doi.org/10.1103/PhysRevResearch.2.023325

[284] Namarvar O F, Missaoui A, Magaud L, Mayou D and de Laissardière G T 2020 *Physical Review B* **101** 245407 URL https://journals.aps.org/prb/abstract/10.1103/PhysRevB.101.245407

[285] Nakatsuji N and Koshino M 2022 *Physical Review B* **105** 245408 URL https://doi.org/10.1103/PhysRevB.105.245408

[286] Forsythe C, Zhou X, Watanabe K, Taniguchi T, Pasupathy A, Moon P, Koshino M, Kim P and Dean C R 2018 *Nature Nanotechnology* **13** 566–571 URL https://doi.org/10.1038/s41565-018-0138-7